UNITED NATIONS EDUCATIONAL, SCIENTIFIC AND CULTURAL ORGANIZATION
INTERNATIONAL ATOMIC ENERGY AGENCY
INTERNATIONAL CENTRE FOR THEORETICAL PHYSICS
I.C.T.P., P.O. BOX 586, 34100 TRIESTE, ITALY, CABLE: CENTRATOM TRIESTE

H4.SMR/1011 - 19

Fourth Workshop on Non-Linear Dynamics and Earthquake Prediction

6 - 24 October 1997

Scaling Organization of Fracture Tectonics. Scaling and Predictability

J.-L. LE MOUEL

Institute de Physique du Globe de Paris
Paris, FRANCE

Energetic balance in scaling organization of fracture tectonics

Claude J. Allègre*†,Pierre Shebalin[a], Jean-Louis Le Mouël*, Clément Narteau*

July 2, 1997

[a] *International Institute of Earthquake Prediction Theory and Mathematical Geophysics, Warshavskoye shosse, 79, korp. 2, 113156 Moscow, Russia*
* *Institut de Physique du Globe de Paris, 4, Place Jussieu, 75252 Paris Cedex 05, France*
† *Université Paris VII, 2, Place Jussieu, 75252 Paris Cedex 05, France*

Corresponding author :

Jean-Louis Le Mouël
Institut de Physique du Globe de Paris
4, Place Jussieu
75252 Paris Cedex 05
France
tel : 01.44.27.39.04
fax : 01.44.27.33.73
e-mail : lemouel@ipgp.jussieu.fr

Abstract

This paper presents a development of the seismicity model S.O.F.T. (scaling organization and fracture tectonics). We remain in the frame of this simple model, which is based on an energy splitting combined with a renormalization group approach. Redistribution of energy over the entire considered domain after strong events was introduced in the previous model. The present version displays some general features of real seismicity, such as Gutenberg-Richter law, Omori law of temporal decrease of the aftershock activity, seismic cycle ("quiet" periods with a background seismic activity, periods of foreshock and aftershock activity). This is shown by numerical experiments in both the single domain case and in the case of exchange of energy between several domains.

1 Introduction

We consider an hierarchy of scales in a fault zone (King, 1983). The earthquake is a critical phenomenon which takes place when fracturing becomes coherently self-organized at different scales (Allègre et al., 1982;Allègre et al., 1995; Ito and Matsuzaki, 1990; Keilis-Borok, 1990). The fault zone is modeled by a domain which permanently receives some energy from outside. This energy is then dissipated through fracturing at different scales. Probabilities of fracturing at different scales are determined using a kind of renormalization group technique (Wilson, 1979) which we named scaling technique (Allègre et al., 1982; Turcotte, 1992). At the lowest (most detailed) scale, this probability is a function of the density of energy per surface (volume) unit. Each rupture causes a total loss of energy in the corresponding part of the domain (Allègre et al., 1995; Kanamori and Anderson, 1975). Later the "lost" part of the domain is gradually reloaded due to the redistribution of energy through slow deformation (creep : King, 1978; Kranz, 1979).

In the frame of the present model the scenario of occurrence of strong earthquakes in a domain is as following. During a quiet period the energy coming from outside increases little by little the probability of fracturing. Only the smallest events occur. At some moment the system starts the coherent fracturing over lowest to medium scales. This is expressed in foreshock activity. When the coherent self-organization achieves the highest scales, a strong earthquake occurs. As a result, a big part of the volume of the domain looses its energy. This diminishes the size of the remaining sound (effective) volume. As a consequence, the process cannot any more reach the highest level scales, and only less strong earthquakes can occur. Part of the released energy is passed to the remaining effective volume in which the density of energy and the fracturing probability increase. This starts the aftershock activity. Simultaneously the redistribution of energy by means of creep is started. Although this process is slow, it is enough to diminish step by step the density of energy. This forces a gradual slowing-up of the aftershock sequence. Finally, the fall of the density of energy passes some limit, the reloading process starts, and the cycle repeats itself (Blanter and Shirman, 1997).

The balance of energy in such a system can also be so that all the received energy has the time to dissipate at intermediate-level scales, giving raise only to moderate magnitude earthquakes. But a small additional energy can lead to the occurrence of a strong earthquake. To model such a behavior we consider later a multidomain case; in this more complex model additional injections of energy, due to exchanges between the domains, are added to the constant rate of energy which is provided to the considered domain from outside. The intensity of those injections is not permanent in time.

In the previous paper on S.O.F.T. model (Allègre et al., 1995) we started with similar energy considerations. But we concentrated on the analysis of the

behavior of the system during a time interval including a strong earthquake, rather than an entire cycle. The weakness was in the aftershock sequences.

In the present paper we introduce a redistribution of energy over the entire domain by a creep mechanism. This allows us to obtain more realistic aftershocks sequences, with a temporal decrease of their intensity (Omori law), and also to reproduce the entire seismic cycle. We also study here more carefully the Gutenberg-Richter law at different stages of the seismic process.

2 Model of fault zone

As in (Allègre et al., 1995) we model a fault zone by a set of domains which represent neighboring segments of this zone (Fig. 1). This system receives continuously energy from its tectonic environment. Each domain has its own behavior, but in addition, all the domains interact with each other through an exchange of energy in various forms (seismic, elastic, tectonics). We will first develop the theory for one domain, then indicate how to extend the model to the case of interacting domains.

2.1 Theoretical formalism

This formalism resumes the general theoretical basis which was described in the previous paper (Allègre et al., 1995). We shall not describe it in detail, but focus on the changes brought to the model. For the analysis of the state of the chosen domain we consider successive time moments $t, t+1, t+2...$ Our model is deliberately intrinsically discrete, and the time unit is unreducible. Let $E(t)$ be the total energy the domain possesses at the time moment t, $\Delta E(t)$ the amount of energy which the domain receives during the time interval $(t, t+1)$ from outside (from plate tectonics and energy exchange with other domains), and $R(t)$ the energy lost by the domain in earthquakes (fracturing, redistribution of strain, seismic waves and heat generation by non-elastic motions):

$$E(t+1) = E(t) + \Delta E(t) - R(t) \tag{1}$$

We shall call the component $\Delta E(t)$ the loading component of the energy rate, and $R(t)$ the dissipation component. The analysis of the balance, or competition, between loading and dissipation is a basic feature of this paper.

We consider a two-dimensional model. During the continuous process of loading and dissipation of energy, the different parts of the domain become obviously characterized by different densities of elastic energy. We model such an heterogeneity by the following simple assumption: at moment t all the energy of the domain is homogeneously distributed over only a part $S(t)$ of the total surface S_0 of the domain. Thus we assume that the remaining part, $S_0 - S(t)$, has completely lost its elastic energy. If the density of energy per surface unit $E(t)/S(t)$

exceeds some threshold ϵ, then this energy excess can result in generating new cracks and developing ancient cracks by growth.

We use the same scaling technique as in Allègre et al. (1982), Allègre and Le Mouël (1994), Allègre et al. (1995). We divide the considered domain into a hierarchy of embedded grids of (3 x 3) cells. L is the maximum number of levels of this hierarchy. At the lowest scale level (1) we have N elementary cells. The probability $p_1(t)$ of fracturing for each elementary cell depends on the excess of the energy density:

$$p_1(t) = \frac{n_1(t)}{N(t)} = 1 - exp(-\alpha(\frac{E(t)}{S(t)} - \epsilon)) \tag{2}$$

$n_1(t)$ being the number of elementary cells where a crack is created during the time interval $(t, t+1)$, α a coefficient. This formula is a natural generalization of the linear one we used in the previous paper.

At the next scale (level 2) we consider $N/9$ cells comprising (3x3) elementary cells. At level 3 we have $N/9^2$ cells comprising (3x3) cells of level 2 etc. From the level k to the level $k+1$ the fracturing is transmitted according to the following rule: if at least three cells of level k alined along the fault zone major axis are cracked, then the corresponding cell of level $k+1$ is also cracked (Fig. 2). We do not introduce any time delay for transmitting fracturation from level k to level $k+1$ (but the whole process of going through all the scales is made during the chosen unit of time). Thus, as in Allègre and Le Mouël (1994), the probability of fracturing at level k during the time interval $(t, t+1)$ is defined recursively as:

$$p_k(t) = P[p_{k-1}(t)] \tag{3}$$

with

$$P(x) = 3x^3(1-x)^6 + 18x^4(1-x)^5 + 45x^5(1-x)^4 \\ +57x^6(1-x)^3 + 36x^7(1-x)^2 + 9x^8(1-x) + x^9$$

We consider the fracturation of one cell at level k during the time interval $(t, t+1)$ as an earthquake occuring at time t (or micro-earthquake for lower levels). The magnitude of this earthquake is naturally proportional to the level k. We shall discuss this in more detail later. The fracturing at the highest level L is the strongest possible earthquake in the considered domain (Aki, 1984); this highest level can be reached only if the current effective surface $S(t)$ of the domain is close to the total surface S_0. In a general way we suppose that only the part $S(t)/S_0$ of all cells can generate quakes; more precisely, the number of earthquakes (micro-earthquakes) of level k which occur during the time interval $(t, t+1)$ is defined as:

$$K_k(t) = [p_k(t) N_k \frac{S(t)}{S_0} + \delta] \tag{4}$$

where $N_k = N/9^{k-1}$ is the total number of cells of level k; [] means integer part; δ is constant ($\delta < 1.0$). The formula (4) controls the maximum level which the system can reach at time t. This replaces a little bit more artificial approach in the previous paper.

We assume as earlier that the energy r_k released in one earthquake at level k is proportional to the linear size of the corresponding cell at the 3^{rd} power, $r_k = \lambda 3^{3k}$ (λ being a scaling parameter). Combining with (4), we obtain the dissipation component of the energy:

$$R(t) = \lambda \sum_{k=1}^{L} K_k(t) 3^{3k} \tag{5}$$

As in S.O.F.T.1, we assume that, after earthquakes have occured, the corresponding subdomains have completely lost their energy. The part of this energy which has not been lost in elastic waves, or heat, has gone to the remaining part of the domain. This process is assumed to need some time to be completed. The size of the effective surface is reduced by a certain amount $\Delta S_1(t)$:

$$\Delta S_1(t) = \mu \sum_{\tau=t-\sigma_1+1}^{t} \frac{R(\tau)}{\sigma_1} \tag{6}$$

where μ is scaling parameter, and σ_1 defines the delay, $\sigma_1 \geq 1$.

As the most significant change of the model in comparison with the previous one, we introduce here a slow redistribution of energy in the entire domain. After Blanter et al. (1996), we suppose the creep being the mechanism of this redistribution.

Energy comes continuously to the domain from outside, and part of it goes to the destroyed subdomains. In addition, through comparatively very slow movements (creep), strains are redistributed so that parts of the destroyed subdomains are reloaded faster than simply due to the external energy injection. This results in the apparent regeneration of the effective surface with the rate $\Delta S_2(t)$. In reality this means only that the distorted subdomains take away some energy from the subdomains in which the concentration of energy is high.

The apparent effective surface regeneration rate $\Delta S_2(t)$ should depend on the relative size of $S(t)$. We take :

$$\Delta S_2(t) = \frac{S_0 - S(t)}{\sigma_2} \tag{7}$$

where we suppose $\sigma_2 \gg \sigma_1$.

Finally the evolution of the effective surface $S(t)$ results from a competition between reduction and increase:

$$S(t+1) = S(t) - \Delta S_1(t) + \Delta S_2(t) \tag{8}$$

Remark: Redistribution of energy (through the creep) consumes some energy. For simplicity we assume that this energy rate is constant (i.e. that its variations are negligibly small in comparison with both loading and dissipation components in (1) (which implies that the constant part of the creep energy is subtracted from the loading component ΔE).

Now we can qualitatively describe how the model generates self-organized critical phenomena similar to the tectonic earthquakes. We can summarize its behaviour in the following way.

The domain permanently receives energy from outside. This energy input increases the energy density per surface unit at elementary (level 1) for cells which form the "effective surface". This increases the probability of fracturing at this level, and consequently the number of micro-earthquakes of level 1. When the probability $p_1(t)$ is lower than the critical value (see Fig. 3) the probabilities $p_k(t)$ are close to 0 for the upper levels of our scale hierarchy $k = 2, 3, ..., L$. When $p_1(t)$ comes close to the critical probability, coherent fracturing reaches upper levels, and foreshock activity starts. Finally $p_1(t)$ passes the critical value, and a strong earthquake (of the highest level L) occurs. A big part of the energy which the system had accumulated before is lost due to the strong earthquake; but the effective surface also falls down, although more slowly due to the time constant σ_1, and the energy density in the remaining part of the domain can increase again, resulting in an increase of $p_1(t)$. This generates the sequence of aftershocks. Their number per time unit is high at the beginning. But, due to the redistribution of the energy through creep, the density of energy per surface unit rapidly falls down, and the aftershock activity decreases. At the end of the cycle the long process of reloading starts and it continues until the new perturbation.

The behavior of the system varies despondently on the values of the parameters. We shall see different examples in the numerical experiments later on. We shall consider first the simple case of the single domain with a constant value $\Delta E(t) = \Delta E_0$ of the rate of loading. In the multidomain case we will simplify the approach proposed in Allègre et al., 1995. Only one domain is considered, but $\Delta E(t)$ contains a time varying component formed by the sum of energy supplies coming from its neighboring domains:

$$\Delta E(t) = \Delta E_0 + \sum_i m_i R_i(t) \tag{9}$$

Index i marks the different domains, $R_i(t)$ is the dissipation energy (5) of domain R_i. In numerical experiments we can iteratively use different realizations of $R_i(t)$ obtained in previous single domain and multidomain cases.

2.2 Gutenberg-Richter law

In real seismicity the distribution of earthquake magnitudes follows the Gutenberg-Richter law (Kanamori and Anderson, 1975):

$$\log(N) = -bM + const, \tag{10}$$

where N is the number of earthquakes with magnitude M during some (rather long) time interval, b the slope of the magnitude-frequency graph. The parameter b varies in the range of 0.6-1.4 according to the different seismic zones (Gutenberg and Richter, 1954; Utsu, 1965; Hattori, 1974). The b value can also vary in time; in addition, the magnitude-frequency graph can have a downward bend at large magnitude values, and this bend can also vary in time. Those effects are interesting when analysing the different stages of the seismic process and its predictability (Narkunskaya and Shnirman, 1990).

To construct magnitude-frequency graphs we have first to define the earthquake magnitude in our model. We mentioned above that the magnitude should be a linear function of the level of the hierarchy of scales k. Magnitude is indeed characteristic of the size of the earthquake; the relationship between the magnitude and the focal surface S is well known (Utsu, 1961):

$$M = C\log(S) + const \tag{11}$$

The coefficient C varies from 0.6 to 1.4 according to the different authors (Okal and Romanowicz, 1994); the most commonly used value is $C = 1$.

In our model we can consider the focal surface to be proportional to the size of the cell of each level k of hierarchy. Thus,

$$M = C\log(\frac{S_0}{N}9^{k-1}) + const = C\log(9k) + const \tag{12}$$

Taking $C = \frac{1}{\log(9)} = 1.05$, we have

$$M = k + const \tag{13}$$

This allows us to use directly k for the earthquake magnitude.

Now we can theoretically construct the magnitude-frequency graphs corresponding to different values of the elementary probability $p_1(t)$ by taking the logarithm of (4) and using (13). Results are shown on Fig.4. We consider one elementary time interval and take $S(t) = S_0, L = 15, \delta = 0.1$. If $p_1(t) \geq 0.6823$ (the critical value: P(0.6823) = 0.6823), the magnitude-frequency graph is practically linear with the slope $b = \log 9 = 0.95$. For lower values of p_1 the graphs have a downward bend which starts at lower values of k the lower is p_1. Examples of magnitude-frequency graphs for longer time intervals will be given later in the numerical experiments.

2.3 Numerical experiments

As in the previous paper, we will examine both single domain and multiple domain cases. In the case of a single domain we will present one example which gives results similar to real seismicity data (Scholtz, 90), then consider the influence on these results of varying the parameters of the model. Afterwards, considering two multidomain examples, we will examine the interaction of neighboring domains and demonstrate the possibility of earthquake triggering.

2.3.1 Single domain case

The modifications of the S.O.F.T. model described above allow us to obtain more realistic aftershock sequences and also to obtain a repetition of strong earthquakes (seismic cycle). This is demonstrated by a typical numerical experiment for the single domain case (Fig. 5 to Fig. 8) in which we used the following values of the parameters: $E_0 = 2.5\,10^6, \Delta E_0 = 2.5\,10^3, \alpha = 6.0\,10^{-7}, \epsilon = 1.5\,10^6, \delta = 0.1, \lambda N = 0.1, \mu = 3.4 \cdot 10^{-7}, \sigma_1 = 3, \sigma_2 = 1000, L = 15$. On Fig. 9 we present in addition the most interesting examples obtained by varying the parameters.

Repetition of strong earthquakes (Fig. 5) (Scholtz, 1982) is due to the balance between the energy coming from outside (integral of ΔE) and the energy dissipated through earthquakes (integral of R). In our typical experiment, the first and strongest (highest hierarchy level L) earthquake occurs at the end of the first loading interval. Afterwards the system is periodically reloaded and produces periodically strong events of level $(L-1)$; the surface S which can generate earthquakes does not reach again the value which is necessary for earthquakes of the maximum level of hierarchy (L) to occur.

The system is strongly self-organized, and its behavior remains the same in a wide diapason of parameters. For example, the balance of coming and dissipated energy remains if the value of ΔE_0 is decreased by a factor of two (Fig. 9b). In this new example the slow rate of coming energy allows the system to completely retrieve its initial state , and we observe a repetition of the strongest possible earthquakes.

In the typical experiment strong earthquakes are followed by sequences of *aftershocks* of all magnitudes (Fig. 6). The decrease in time of the number of aftershocks is self-similar (Fig. 8), as in the case of real aftershock sequences (Omori law : Utsu, 1965).

Foreshocks are less strong than aftershocks: in the typical experiment their maximum magnitude corresponds only to the third level of hierarchy from the top (k=13) (Fig. 6). The slope of the magnitude-frequency graph corresponding to the foreshocks sequence is significantly higher than it is for reloading and aftershock phases (Fig. 7).

We have then, as announced supra, studied how varying the parameters affects the behavior of the model. The most interesting examples are shown on Fig. 9.

A change of the initial energy E_0 can only shift the time scale (of course, if it does not immediately provide the critical value of p_t). As in the previous paper (S.O.F.T.1), the most important parameters are ΔE_0 and α (parameter α replaces parameter k in the previous paper).

Very small values of ΔE_0 give an a-seismic behaviour (Fig. 9a). But the level of total energy in this example is high enough (compare with Fig. 5a) to produce the strongest earthquakes, and a small injection of additional energy can generate (trigger) this big event. We will show that later when considering multidomain examples. The opposite situation corresponds to high values of ΔE_0 (Fig. 9c): the strong earthquake largely destroys the domain; after this event only a very small part of the initial surface remains effective; this part generates permanently small events. Intermediate values of ΔE_0 provide a repetition of strong earthquakes as on Fig. 5 and 9b. Fig. 10 shows how the period of this repetition (the seismic cycle) depends on the value of ΔE_0 (all the other parameters being fixed).

Parameter α influences too the period of strong events repetition. Small values correspond to a slower energy dissipation rate and, accordingly, to larger values of this repetition period. Large values of α can produce a picture which seems to represent a discrete case (Fig. 9e : each event seems to be isolated from each other). In reality this is no more than the standard case but with a very short period of the seismic cycle. The decrease in time of the amplitude of R at the beginning is only a transitional period due to the chosen initial conditions.

Influence of parameter ϵ is similar but opposite to that of parameter α; small values of ϵ correspond to short periods of the seismic cycle. The parameter μ also provides longer seismic cycle periods when it is given larger values and produces the pseudo-discrete picture when it is given small values. The value of δ practically does not change the results if it varies in the range 0.05-0.5.

Parameter λ changes the energy scale, and has to be considered simultaneously with parameters $\Delta E_0, \epsilon$ and α. The maximum hierarchy level L has be taken equal to 15 and no other value has been considered.

Larger values of the time delay σ_1, characteristic of the effective surface decrease after an event, can generate a seismic swarm as on Fig. 9f; the aftershocks sequence is replaced by a sequence of strong events of similar magnitude. σ_2 influences the length of the aftershocks sequence and the period of the seismic cycle. One example is shown on Fig. 9g.

2.3.2 Multidomain case

We present here two simple examples of interaction of several domains. The first example represents the possibility of triggering strong earthquakes. The second shows that even a small variability in time of the energy feeding the considered domain can significantly influence its seismicity (Keilis-Borok, 1994). We assume that this variability is produced by an interaction with a neighboring domain

(part of the energy R dissipated in this second domain goes to the domain under consideration).

Earthquake triggering. We consider here the case of a very small rate of energy ΔE_0 (Fig. 9a) and inject into the domain an extra-amount of energy (Fig. 11); the value of this amount is $5\,10^3$, that is approximately 1/200 of the energy of the strongest event. This injection acts as a triggering for generating an event of the highest level L. It is interesting to observe that this event occurs with some delay after the injection and is preceded by foreshocks. The energy of the event is two orders of magnitude higher than the value of the injected extra-amount of energy.

Interaction of neighboring domains. Let us consider two domains (Fig. 12). In the first domain the parameters of the model are the same as in the typical experiment except for $E_0 = 1.5\,10^6$ and $\epsilon = 1.2\,10^6$. The graph representing the rupture energy R for this case (without interaction) is shown on Fig. 12a. The second domain is exactly as in the typical experiment. We assume that 1/20 of the rupture energy R of the second domain is transmitted to the first one. The average of this energy (Fig. 12b) per time unit is to $0.17\,10^3$. In order not to change the total energy which comes into the first domain, we subtract from ΔE_0 (corresponding to the first domain) this average value, but at every moment we add the instantaneous energy coming from the second domain. The result (graphs of R and p_1) is shown on Fig. 12c. The interval between strong events is no longer constant.

More complicated combinations of domains with different parameters will lead to more complicated results. We think that practically any sequence of events can be modeled in such a way.

3 Discussion and conclusions

In the present paper we have obtained a significant improvement of the previous S.O.F.T. model. First, we succeeded in obtaining the decrease in time of the number of aftershocks and of their energy, similarly to what is observed in the case of the real earthquakes (Omori law). Secondly, due to the introduction of energy redistribution by creep, we have obtained the repetition of the seismic cycle, with periods of low level of seismic activity, periods of activation (foreshocks), followed by a strong main shock and aftershocks.

We model creep by an apparent reconstruction of the surface of the domain at a rate proportional to the size of the broken area (formula (7)). This can be explained as well in terms of heterogeneity of the energy distribution in the domain : we model this heterogeneity by two homogenous parts of the domain : a broken part, in which the potential energy is zero, and a non broken part, in which the density of potential energy is constant. This is a kind of description of asperity or barrier type (Aki, 1984). In such words, the redistribution of energy

is equivalent to an increase of the size of the unbroken part.

The apparent surface reconstruction we spoke above has nothing to do with the process of consolidation of the broken material. We guess that consolidation process is incomparatively slower.

How does the model work?

Periods of low seismic activity (seismic noise) correspond to the relatively long periods of loading (or reloading) of the system, when the energy comes from outside much faster than it is dissipated by small events. During these periods the density of energy is below the critical value.

As the energy density approaches the critical value, the seismic activity increases. In our model foreshocks start earlier at lower levels of scaling (lower magnitude of events); they may be absent at higher levels. During the foreshock period the energy continues to accumulate, because the foreshocks energy is weak.

Finally, a significant part of the accumulated energy is released in the strong earthquake which breaks part of the domain. The remaining potential energy is passed to the unbroken part (possibly with some small delay). At the beginning the relative losses in area of the sound domain are higher than the relative losses of energy. This gives a further increase of the energy density, and aftershocks start. The number per unit time and energy of the quakes are now limited by the size of the unbroken part of the domain. The energy released by aftershocks is enough for the total density energy of the system continue to drop down. The "working" surface at some point stabilizes - when losses of the sound surface become equal to the apparent recovering of surface by creep. Those two processes together lead to a decreasing of the energy density. At some moment this density drops below the critical value, and the aftershock sequence transforms into seismic noise (we have to note that in the present model the beginning of the aftershock sequence is accompanied by an increase of the energy concentration).

Thus, the frame of this model, characterized by a reasonnably small number of parameters, has provided in numerical experiments a behavior presenting some gross properties of real seismicity: Gutenberg-Richter law, Omori law, seismic cycle.

Let us emphasize again a main characteristic of the model : tectonic energy enters it at the smallest scale and cascades up to larger scale levels. This is compatible with the asperities mechanism as defined by Aki (1984) : asperities represent smaller scale heterogeneities than the whole fault plane, and the process creating asperities involves foreshocks and precursing creep; the fault plane becomes heterogeneous before the rupture and the main shock is a stress smoothing process over the fault plane. But, as pointed out by one of the referees, the barriers mechanism rather calls for a cascading down of energy. Barriers, as defined by the same paper of Aki (1984), represent small scale heterogeneities created by the main shock rupture. Non-uniform slip over the fault plane creates stress concentration over it, causing aftershocks along the mainshock rupture plane. The main rupture is in this case a stress roughening process, and smaller events

are created by larger events. Tectonic energy enters the system from the largest scale, through plate motion, and is cascaded down to smaller scales.

Both cascading up and down may be simultaneously working in the actual fault zone, but, according to the referee, observations support the evidence of cascading down. For example, he says, foreshocks are subtle and rare phenomena, while aftershocks are ubiquitous and robust. But this one observation does not, in our opinion, contradict the inferences of the present model: foreshocks are often present only at the smallest scales and then have very small energy, whereas aftershocks are ubiquitous and much more energetic (section 2.3.1) even wihtout introducing cascading down. Nevertheless cascading down is certainly to be introduced into the model, without giving up its main ingredient, i.e. large scale self organization from small scale events. This will be one of our next steps. Together with the introducing of other physical concepts, like nucleation and growth, and heterogeneities, it will allow us, we hope, to closer approach the rupture dynamics and to account for more observations on earthquakes than the Gutemberg-Richter and Omori law.

AKNOWLEDGEMENTS

We thank the referees for judiciouscomments. The present work was completed in IPG Paris while P. Shebalin had a visitory scientist grant within the IPG-MITPAN cooperation agreement. The present work was also supported by the Russian Foundation of Fundamental Research (Project Code 93-05-8870) and by INTAS Foundation (Project Code INTAS-93-457). IPGP contribution no. .....

REFERENCES

Allègre, C. J., Le Mouël J.L., Provost A., 1982, Scaling rules i rock fracture and possible implications for earthquake prediction, *Nature*, **297**, 47–49.

Allègre, C.J et J.L. Le Mouël, 1994, Introduction of scaling techniques in brittle fracture of rocks, *Physics of the earth and planetary interiors*, **87**, 85–93.

Allègre, C.J., J.L. Le Mouël, C. Ha Duyen et C. Narteau, 1995, Scaling Organisation of Fracture Tectonics (S.O.F.T.) and earthquakes Mechanism, *Physics of the earth and planetary interiors*, **92**, 215–233.

Aki, K., 1984, Asperities, barriers, characteristic earthquakes and strong motion prediction, *J. Geophys. Res.*, **86**, 5867–5872.

Blanter E.M., Shnirman M.G., Le Mouël J.L., C.J. Allègre, 1997, Scaling laws in blocks dynamics and dynamic self organized criticaly, *Phys. Earth Planet. Inter.*, **99**, 295–307.

Blanter E.M., Shnirman M.G., Le Mouël J.L., Hierarchical model of seismicity: scaling and predictability, *Phys. Earth Planet. Inter.*, (in press).

Blanter E.M., Shnirman M.G., 1996, Self-organized criticality in hierarchical model of defects development, *Phys. Rev. E.*, **53**, 3408

Gutenberg B., Richter C.F., Seismicity of the Earth and associated phenomena, *Princeton Univ. Press, 2nd edition*, **1954**, 310 p.

Hattori S., 1974, Regional distribution of b value in the world, *Bull. Intern. Seismol. and Earth Eng.*, **12**, 39–58.

Ito, K, and Matsuzaki, 1990, Earthquakes as self-organised critical phenomenon, *J. Geophys. Res.*, **95**, 6853–6860.

Kanamori, K., and Anderson, D.L., 1975, Theoretical basis of some empirical relations in seismology, *Seis. Soc. Am. Bull.*, **65**, 1073–1096.

Keilis-Borok, V.I., 1994, Sympthoms of instability in a system of earthquake-prone faults, *Physica D*, **77**, 193–199.

Keilis-Borok, V.I., 1990, The lithosphere of the Earth as a nonlinear system with implications for earthquake prediction, *Rev. Geophys.*, **28, N 1**, 9–34.

King, G.C.P., 1978, Geological Faults : fracture, creep and strain, *Phil. Trans. R. Soc. Lond.*, **A. 288**, 197–212.

King, G.C.P., 1983, The accomodation of large strains in the upper lithosphere of the Earth and other solids by self-similar fault system : the geometrical origin of the b-value, *Pageoph*, **121**, 567–585.

Kranz R.L., 1979, Crack growth and development during creep of Barre granite, *Int. J. Rock Mech. Min. Sci.*, **16**, 23–35.

Narkunskaya G.S., Shnirman M.G., 1990, Hierarchical model of defects development and seismisity, *Phys. Earth Planet. Inter.*, **61**, 29–35.
200–216.

Okal, E. A. and B.A. Romanowicz, On the variation of b-values with earthquake size, *Phys. Earth Planet. Inter.*, **87**, 55–76.

Scholtz, C.H., 1982, Scaling laws for large earthquakes : consequences on physical models, *Bull. Seism. Soc. Am.*, **72**, 1-14.

Scholtz, C.H., 1990, The mechanics of earthquakes and faulting, *Cambridge University Press*, United Kingdom.

Turcotte D.L., 1992, Fractals and Chaos in geology and geophysics, *Cambridge University Press*, United Kingdom.

Utsu T., 1965, Aftershocks and earthquake statistics, *J. Fac. Sci. Hokkaido Univ. Ser. VII.* **3**, 379–441.

Utsu T., 1961, Statistical study on the occurence of aftershocks, *Geophys. Mag.*, **30**, 521–605.

Wilson, K.G., 1979, Problems in physics with many scales of length, *Sci. Am.*, **August**, 140–157.

FIGURE CAPTIONS

Fig. 1. Illustration of a model of fault zone. Four domain (separated by a solid line) receive an elastic energy (Δe) from the stress applied to their boudary by plates tectonics. The fault zone is supposed to be composed of a brittle layer above a plastic one. Fat lines represent the major faults, dotted lines represent the minor faults, and dashed lines represent the exchange of energy between two domains. Around each segment, we define a three-dimensional domain with specific geometries, extending to a prescribed depth. The three-dimensional domains are those where the fracture occur.

Fig. 2. This cartoon illustrates the scaling technique derived from the renormalization group theory used by Allègre and Le Mouël (1994). The domain (Fig. A) is divided into subdomains (Fig. B), the subdomains are divided into smaller ones... until the elementary domain scale is reached. We used a grid of $3 * 3$ domains.(Allègre et al, 1995).

Fig. 3. Probability of fracturing at different levels of the hierarchy. This probability is defined by formula (3). All curves intersect at the critical value $p_1 = 0.6823 : p_{k+1}(x) \geq p_k(x)$, if $x \geq 0.6823$.

Fig. 4. Theoretical magnitude-frequency graphs for one elementary time interval and different values of p_1. Hierarchy level k is used as earthquake magnitude according to (13). Graphs are constructed using (4) with $S(t) = S_0, L = 15, \delta = 0.1$.

Fig. 5. Typical experiment in the single domain case; (a) — on a short time span (b) — on a long time span. Time variation of R, p_1, E, and S are shown. In this typical experiment the following parameters of the model are used: $E_0 = 2.5\,10^6, \Delta E_0 = 2.5\,10^3, \alpha = 6.0\,10^{-7}, \epsilon = 1.5\,10^6, \delta = 0.1, \lambda N = 0.1, \mu = 3.4\,10^{-7}, \sigma_1 = 3, \sigma_2 = 1000, L = 15$.

Fig. 6. Time variation of the number of events per unit of time, at different levels of hierarchy, for the typical experiment. Values of the parameters are as for fig. 5.

Fig. 7. Magnitude-frequency graphs for different stages of the seismic process. We take the hierarchy level k as the magnitude according to formula (13). The typical experiment (fig. 5) parameters values are used. The b value for all curves is calculated by the least squares method on the interval $9 \leq k \leq 13$. The slope for foreshocks ($t = 360 - 368$, see fig. 5a) is significantly higher than the slope for aftershocks, the reloading period, and the total considered time interval.

Fig. 8. Self-similarity of aftershock sequences. a) Typical experiment of the model; b) aftershocks $M \geq 4$ of the earthquake 26/5/1983 in Japan, $M = 7.7$; c) aftershocks $M \geq 4$ of the Southern Kurils earthquake 4/10/1994, $M = 8.1$; d) aftershocks $M \geq 2$ of the Landers earthquake 28/6/1992, $M = 6.7$ in California. We consider histograms of the number of aftershocks in the fixed length boxes as function of time after the main shock. Three different time scales (changing like 1,2,4) are shown for each example. The picture for the typical experiment of our model is very similar to those for real aftershock series. Self-similarity of the real

aftershock sequences is due to the Omori law.

Fig 9. Results of varying of the model parameters in comparison with the typical result. The values of parameters are the same as on Fig. 5 except: a) $\Delta E_0 = 0.7\,10^2$, b) $\Delta E_0 = 1.25\,10^3$, c) $\Delta E_0 = 2.85\,10^3$, d) $\alpha = 0.3\,10^{-6}$, e) $\alpha = 0.9\,10^{-6}$, f) $\sigma_1 = 15$, g) $\sigma_2 = 300$.

Fig. 10. The periodicity of strong earthquakes as a function of the parameter ΔE_0. All other parameters are as for Fig. 5. The limit for low values corresponds to the non-stable balance with high accumulated energy. The limit for high values corresponds to the stable balance with accumulated energy and permanent dissipation of energy by small events.

Fig 11. Example of triggering a strong earthquake by a small energy injection. The graph at the top shows a fragment of the graph of R from Fig. 9a. Next graph shows the energy injection. The bottom graph represents values of R when the small energy injection has been added. The value of the injected energy is two orders of magnitude lower than the value of R generated by the top hierarchy level events.

Fig. 12. Interaction of two domains. a) rupture energy R for a domain with the same model parameters as for fig. 5, except: $E_0 = 1.5\,10^6$ and $\epsilon = 1.2\,10^6$; b) rupture energy($.\frac{1}{20}$) in the typical experiment (parameters as on fig. 5); c) resulting rupture energy and p_1 in the first domain.

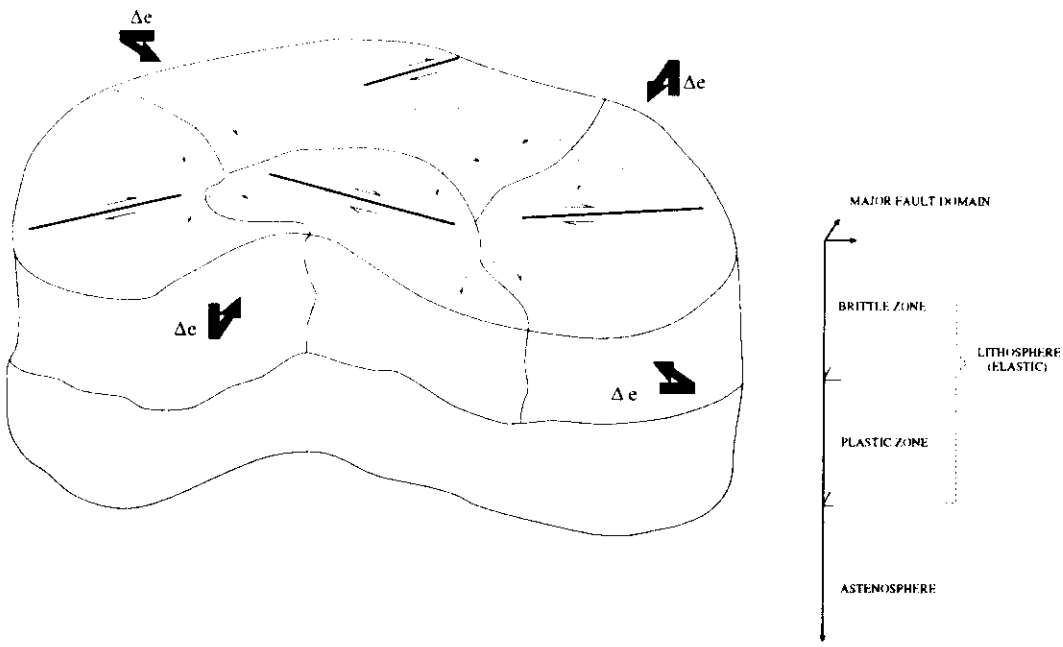
Δe
Δe
Δe
Δe
MAJOR FAULT DOMAIN
BRITTLE ZONE
LITHOSPHERE (ELASTIC)
PLASTIC ZONE
ASTENOSPHERE

Figure 1

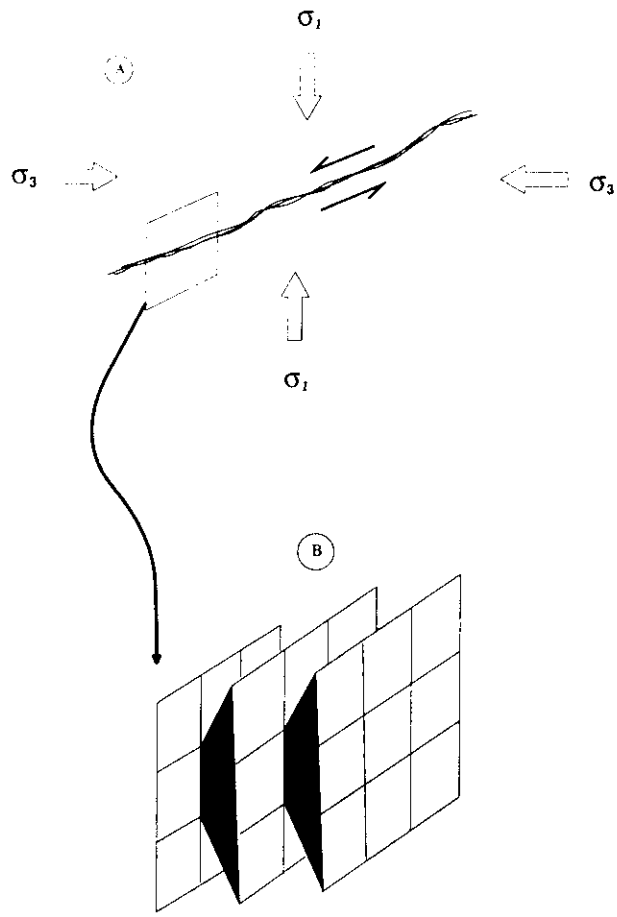

Figure 2

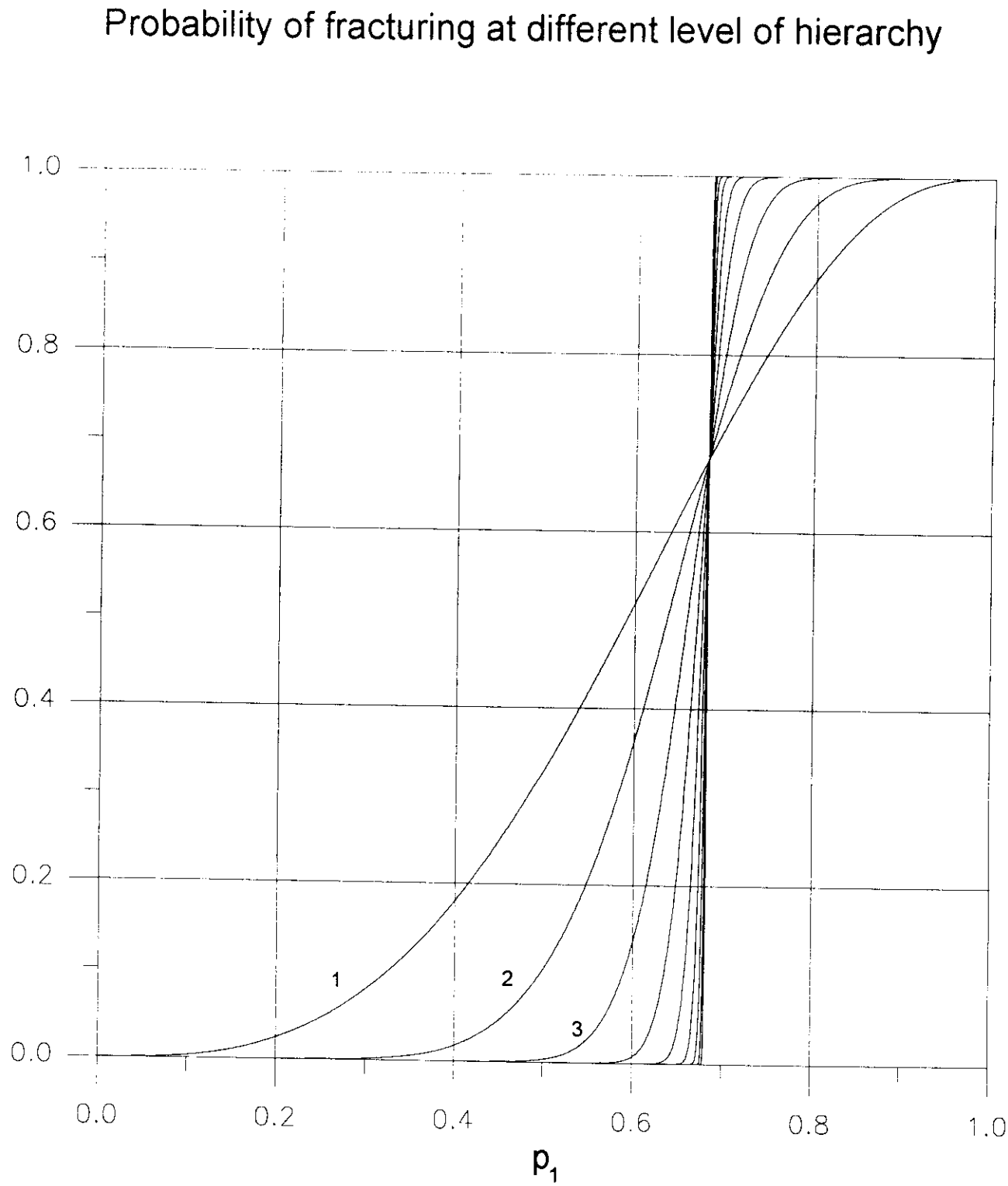
Probability of fracturing at different level of hierarchy
1.0
0.8
0.6
0.4
0.2
0.0
0.0
0.2
0.4
0.6
0.8
1.0
p_1
1
2
3

Fig. 3

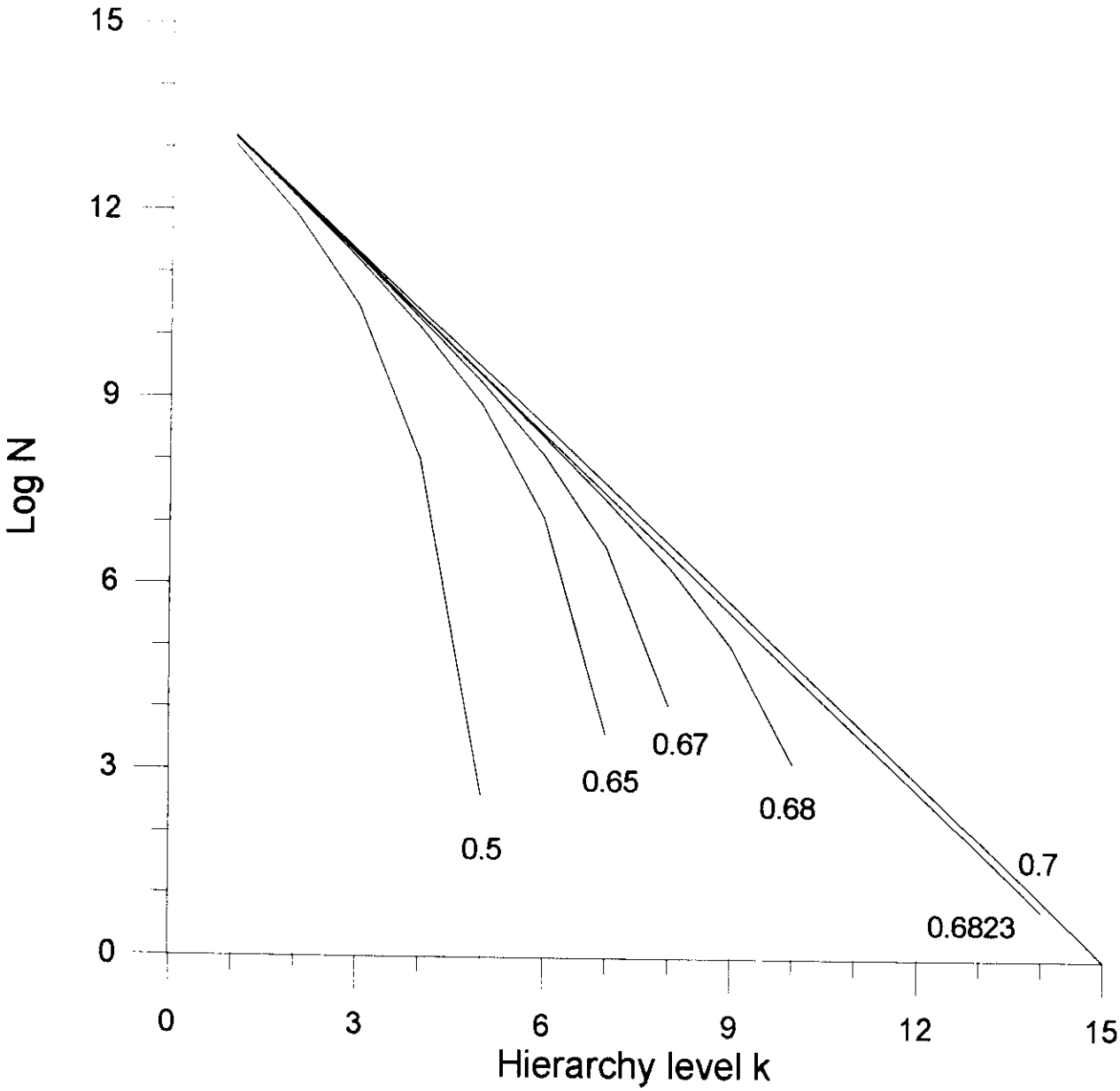
15
12
9
6
3
0
Log N
0
3
6
9
12
15
Hierarchy level k
0.5
0.65
0.67
0.68
0.7
0.6823

Fig 4

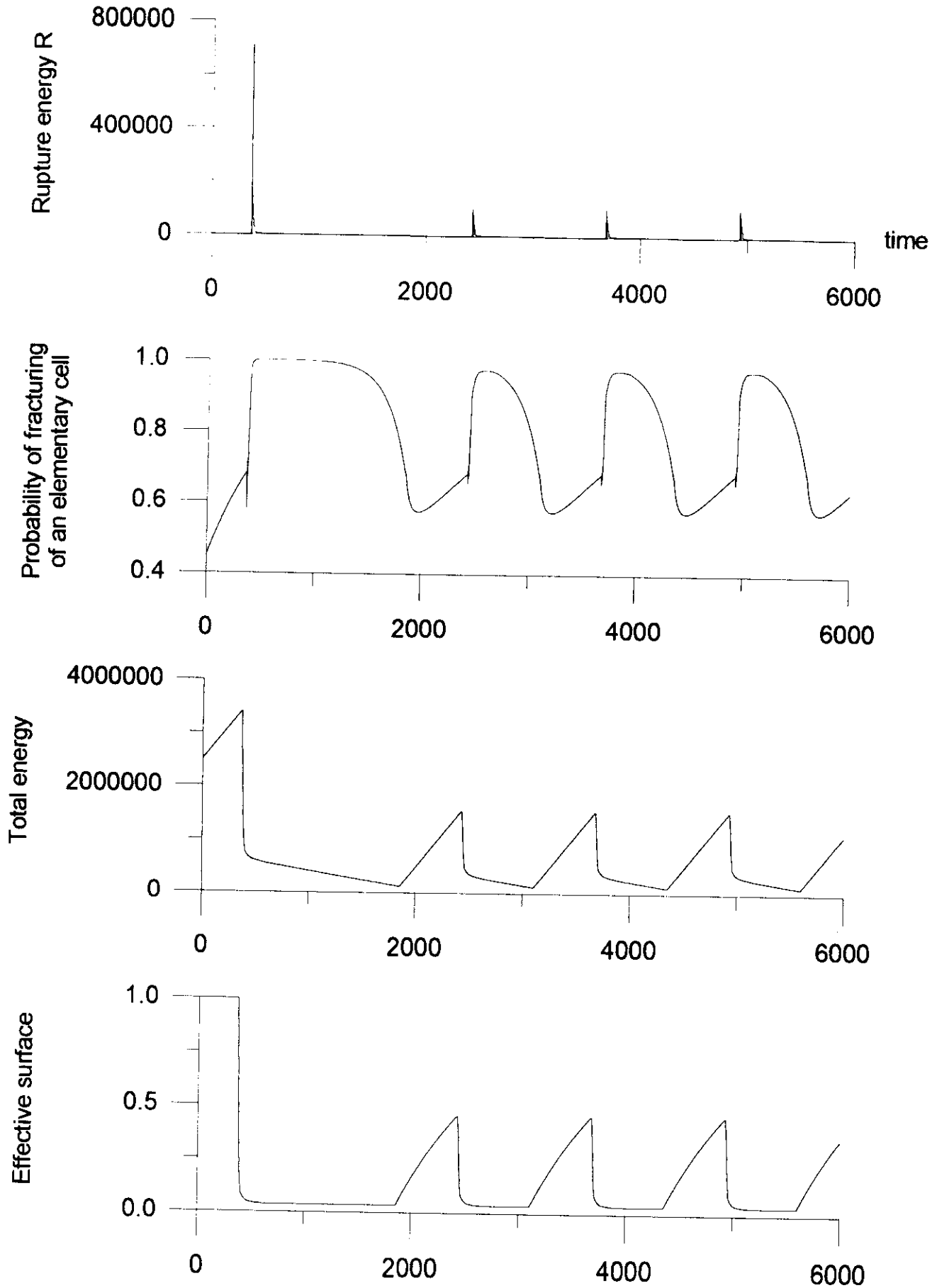
Rupture energy R
800000
400000
0
time
0
2000
4000
6000
Probability of fracturing of an elementary cell
1.0
0.8
0.6
0.4
0
2000
4000
6000
Total energy
4000000
2000000
0
0
2000
4000
6000
Effective surface
1.0
0.5
0.0
0
2000
4000
6000

Fig. 5

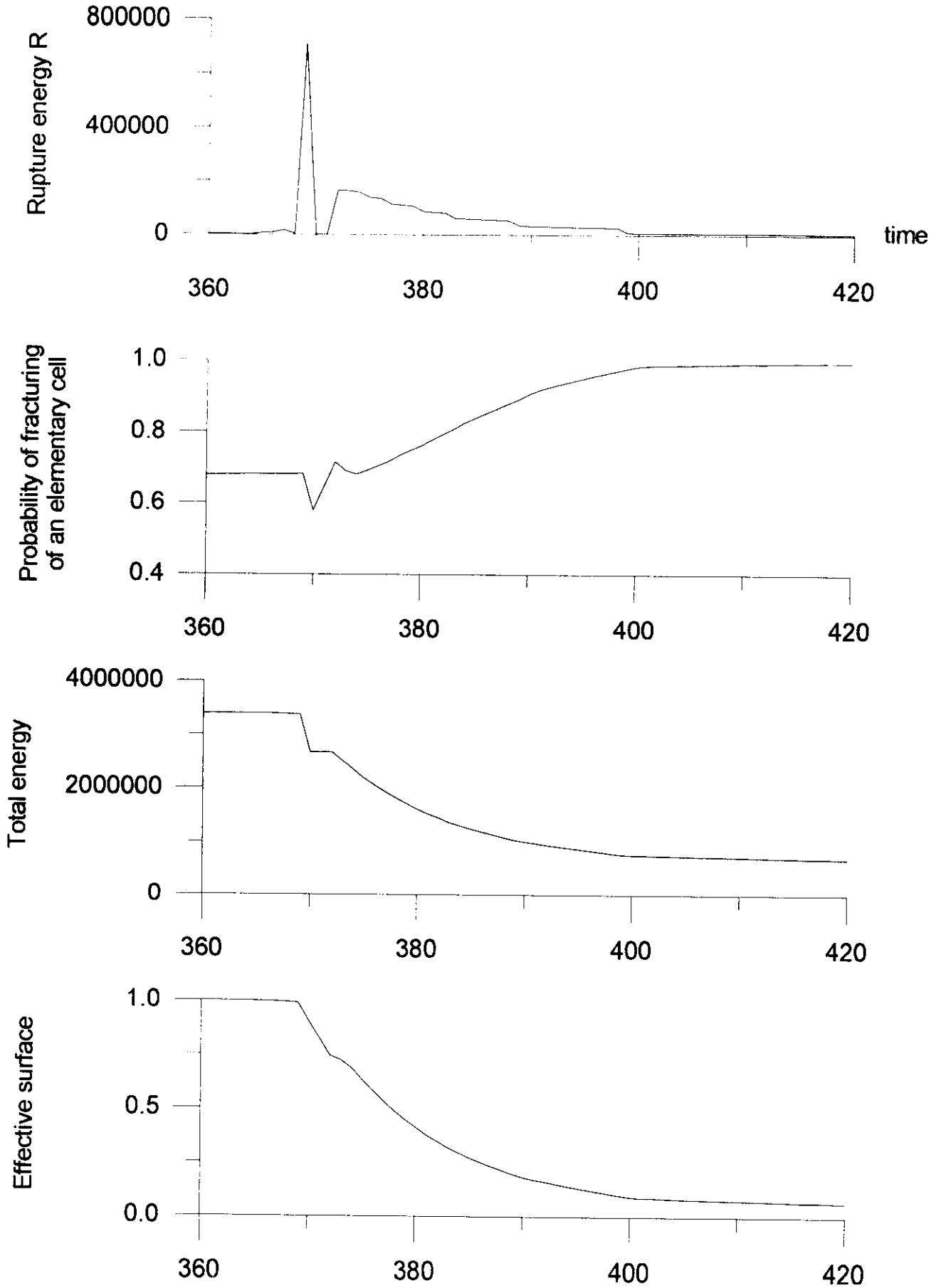
Rupture energy R
800000
400000
0
time
360
380
400
420
Probability of fracturing of an elementary cell
1.0
0.8
0.6
0.4
360
380
400
420
Total energy
4000000
2000000
0
360
380
400
420
Effective surface
1.0
0.5
0.0
360
380
400
420

Fig. 5a

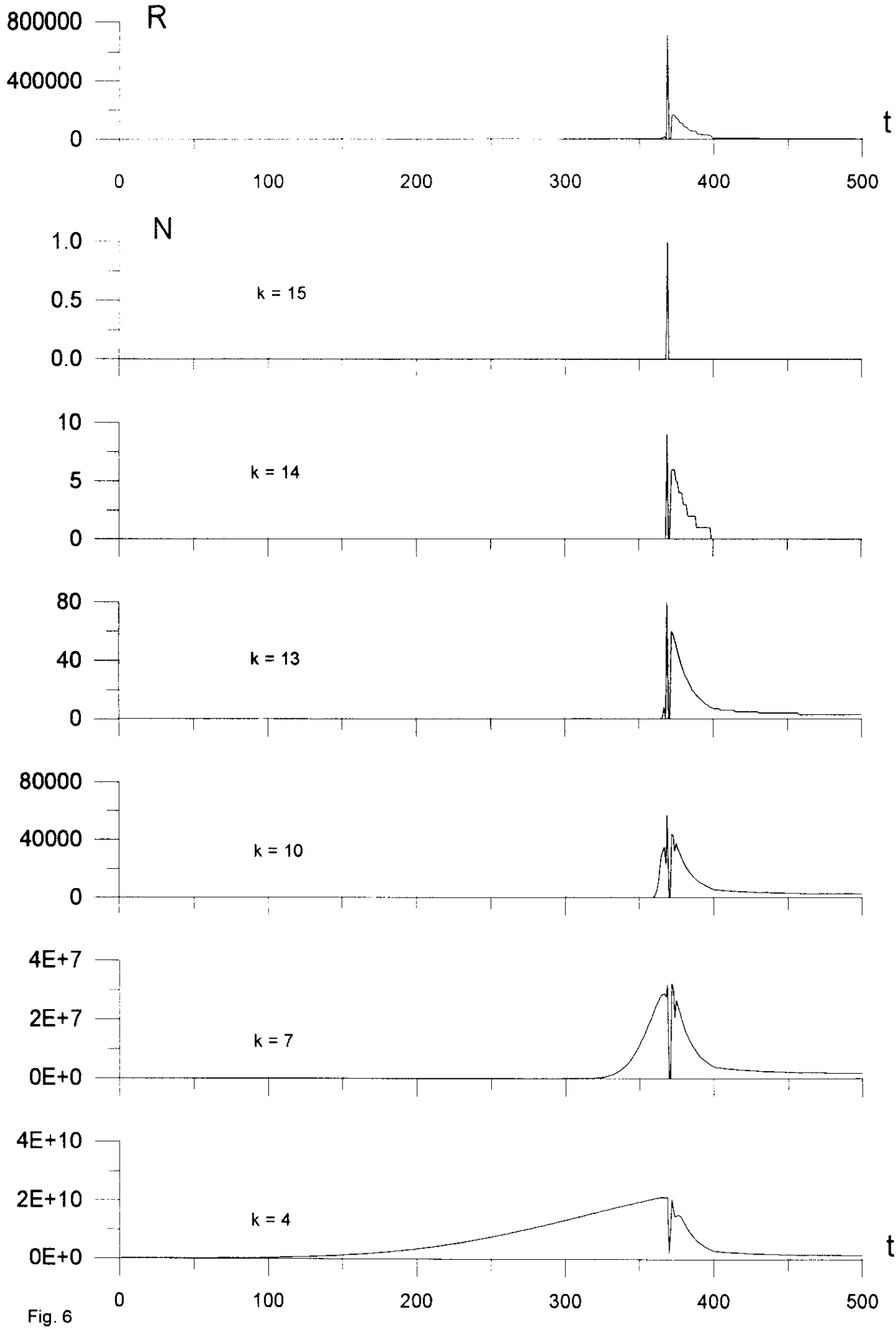
R
800000
400000
0
t
0
100
200
300
400
500
N
1.0
0.5
0.0
k = 15
10
5
0
k = 14
80
40
0
k = 13
80000
40000
0
k = 10
4E+7
2E+7
0E+0
k = 7
4E+10
2E+10
0E+0
k = 4
t
0
100
200
300
400
500

Fig. 6

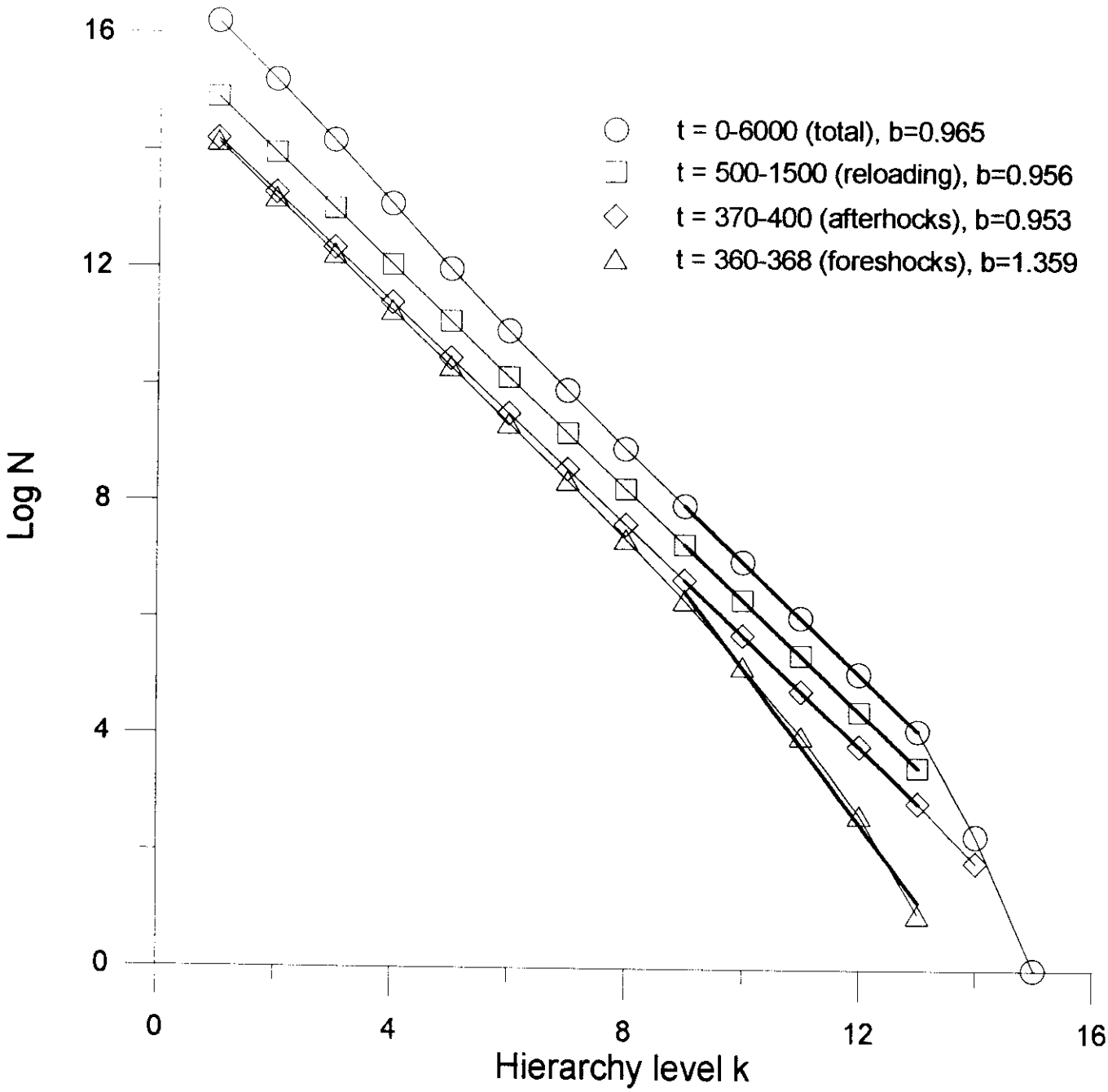
16
12
8
4
0
Log N
0
4
8
12
16
Hierarchy level k
t = 0-6000 (total), b=0.965
t = 500-1500 (reloading), b=0.956
t = 370-400 (afterhocks), b=0.953
t = 360-368 (foreshocks), b=1.359

Fig. 7

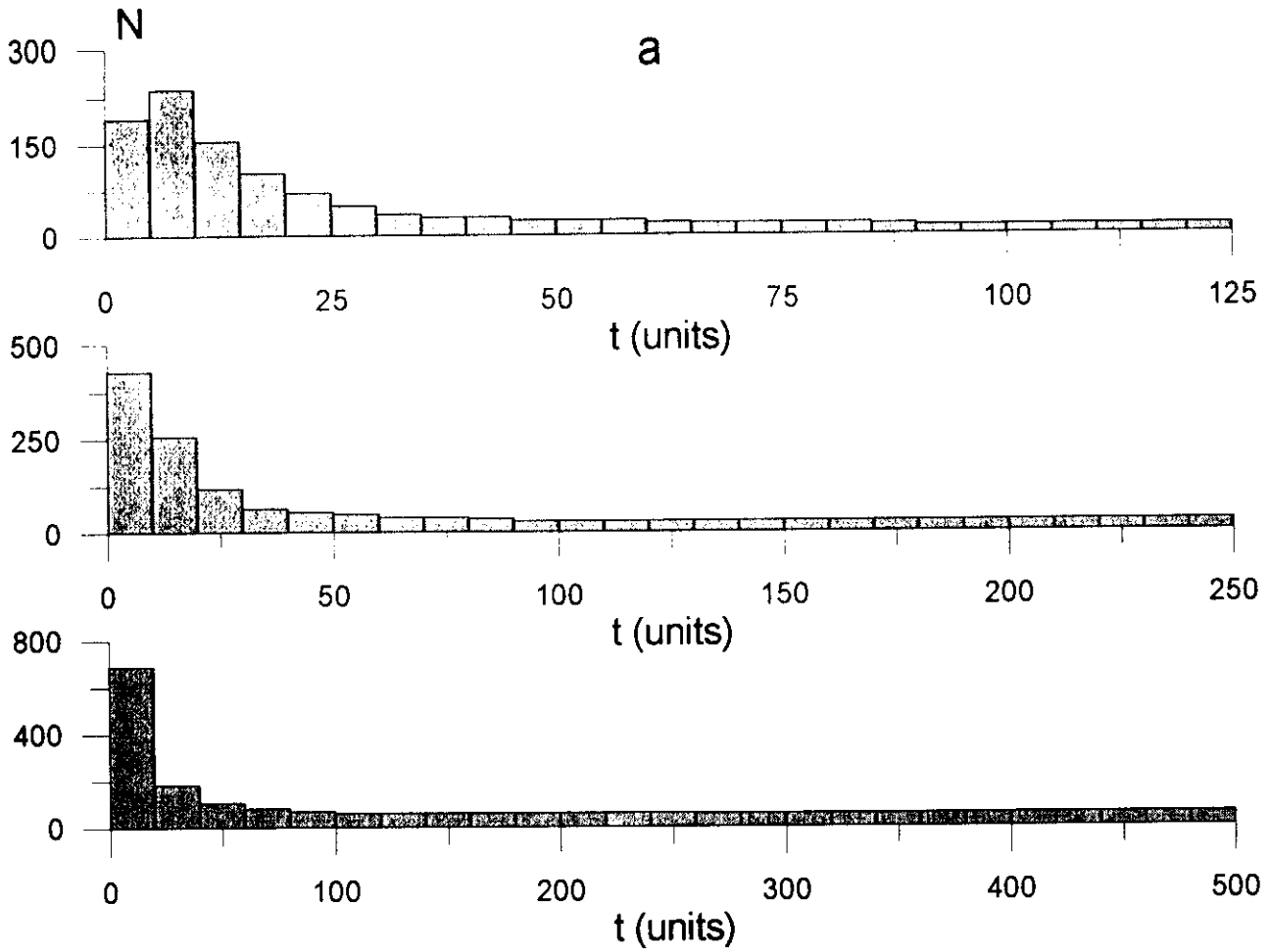
N
a
300
150
0
0
25
50
75
100
125
t (units)
500
250
0
0
50
100
150
200
250
t (units)
800
400
0
0
100
200
300
400
500
t (units)

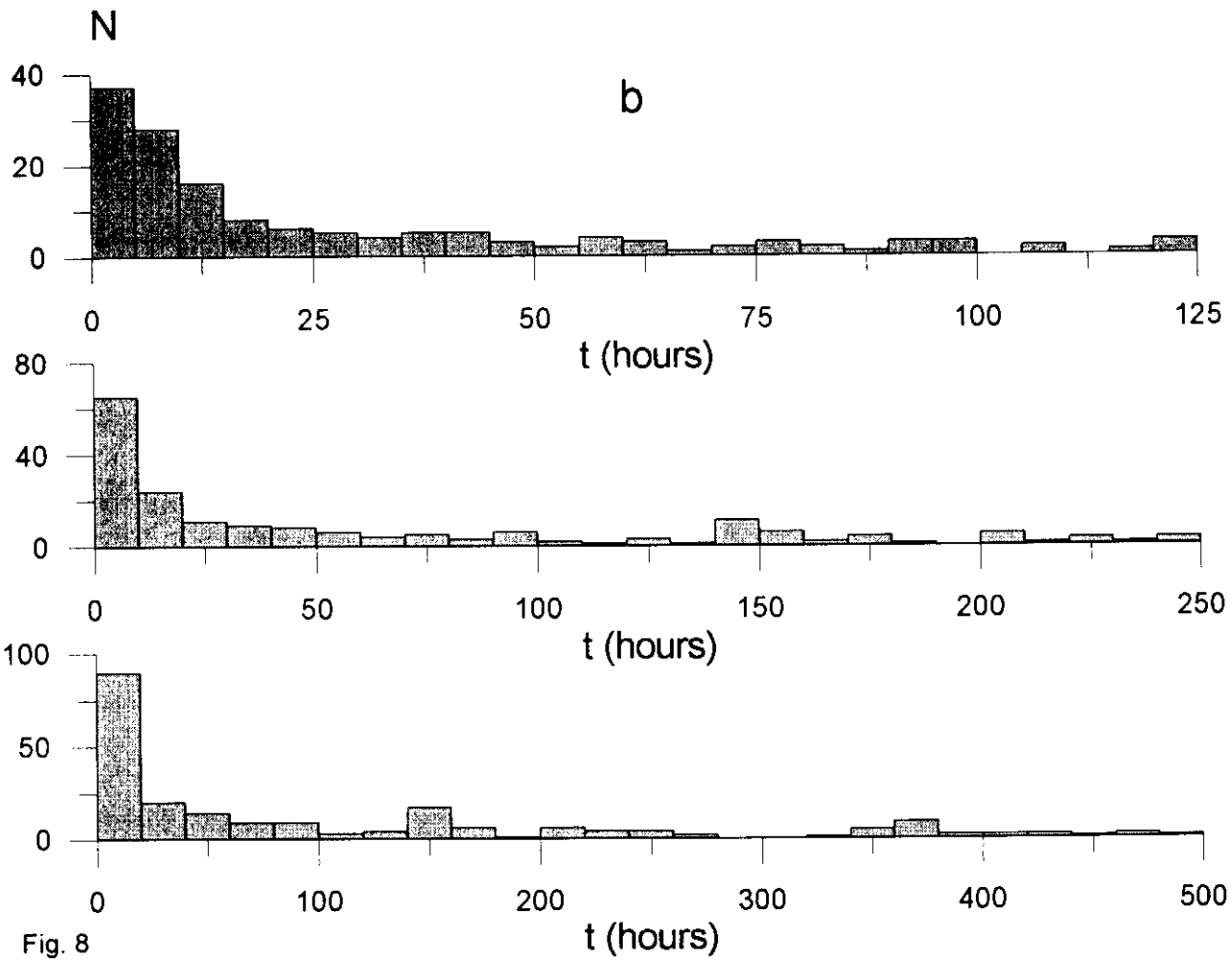
N
b
40
20
0
0
25
50
75
100
125
t (hours)
80
40
0
0
50
100
150
200
250
t (hours)
100
50
0
0
100
200
300
400
500
t (hours)

Fig. 8

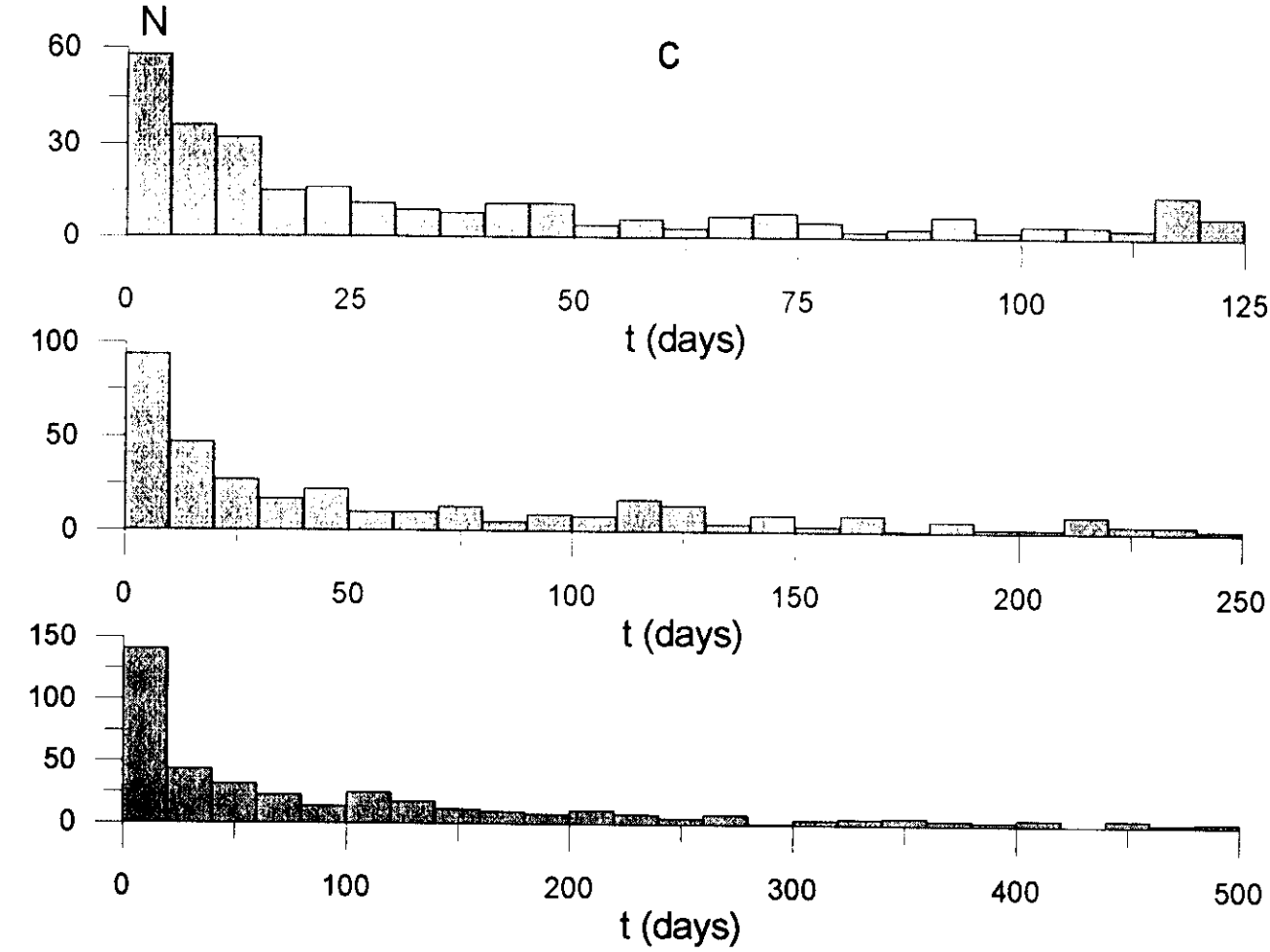
N
c
60
30
0
0
25
50
75
100
125
t (days)
100
50
0
0
50
100
150
200
250
t (days)
150
100
50
0
0
100
200
300
400
500
t (days)

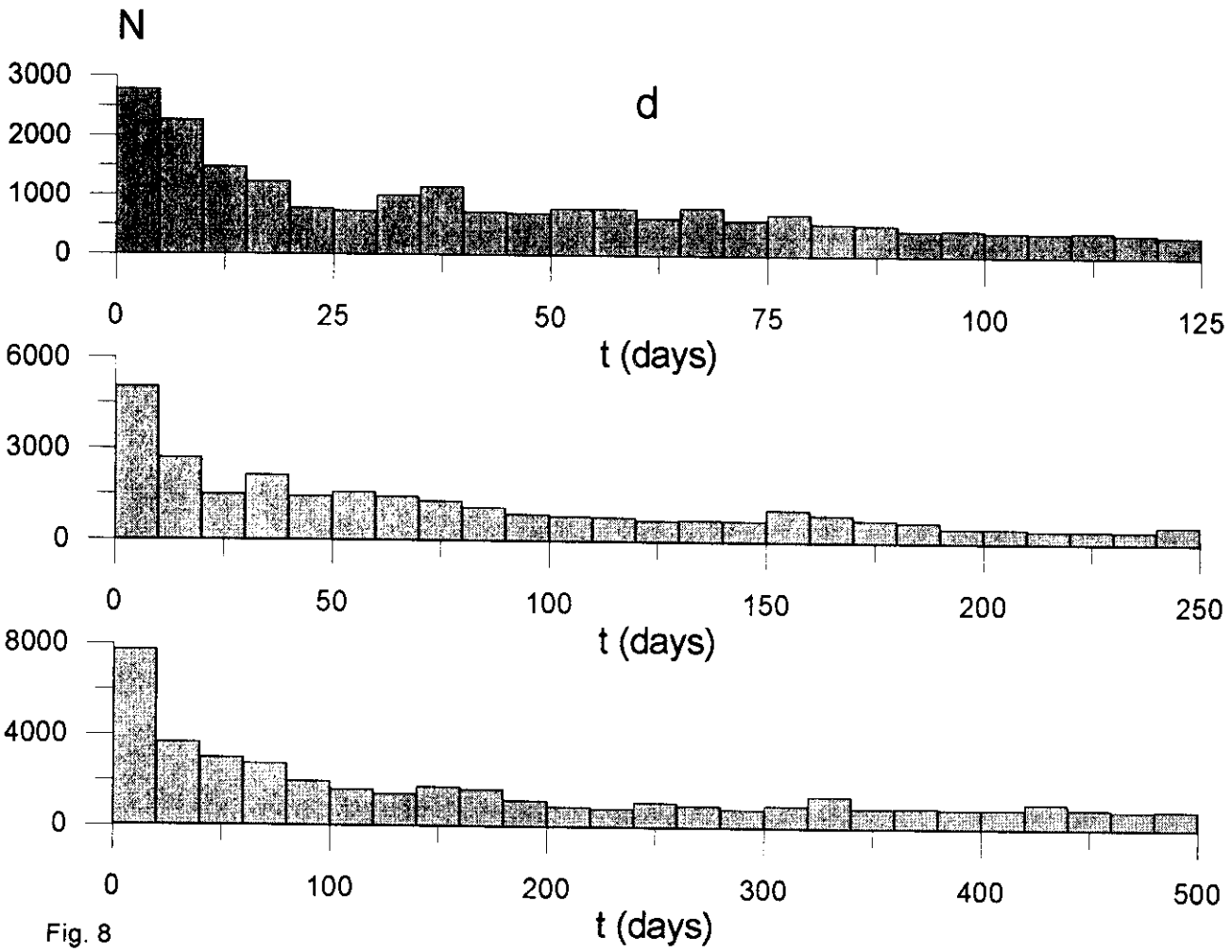
N
d
3000
2000
1000
0
0
25
50
75
100
125
t (days)
6000
3000
0
0
50
100
150
200
250
t (days)
8000
4000
0
0
100
200
300
400
500
t (days)

Fig. 8

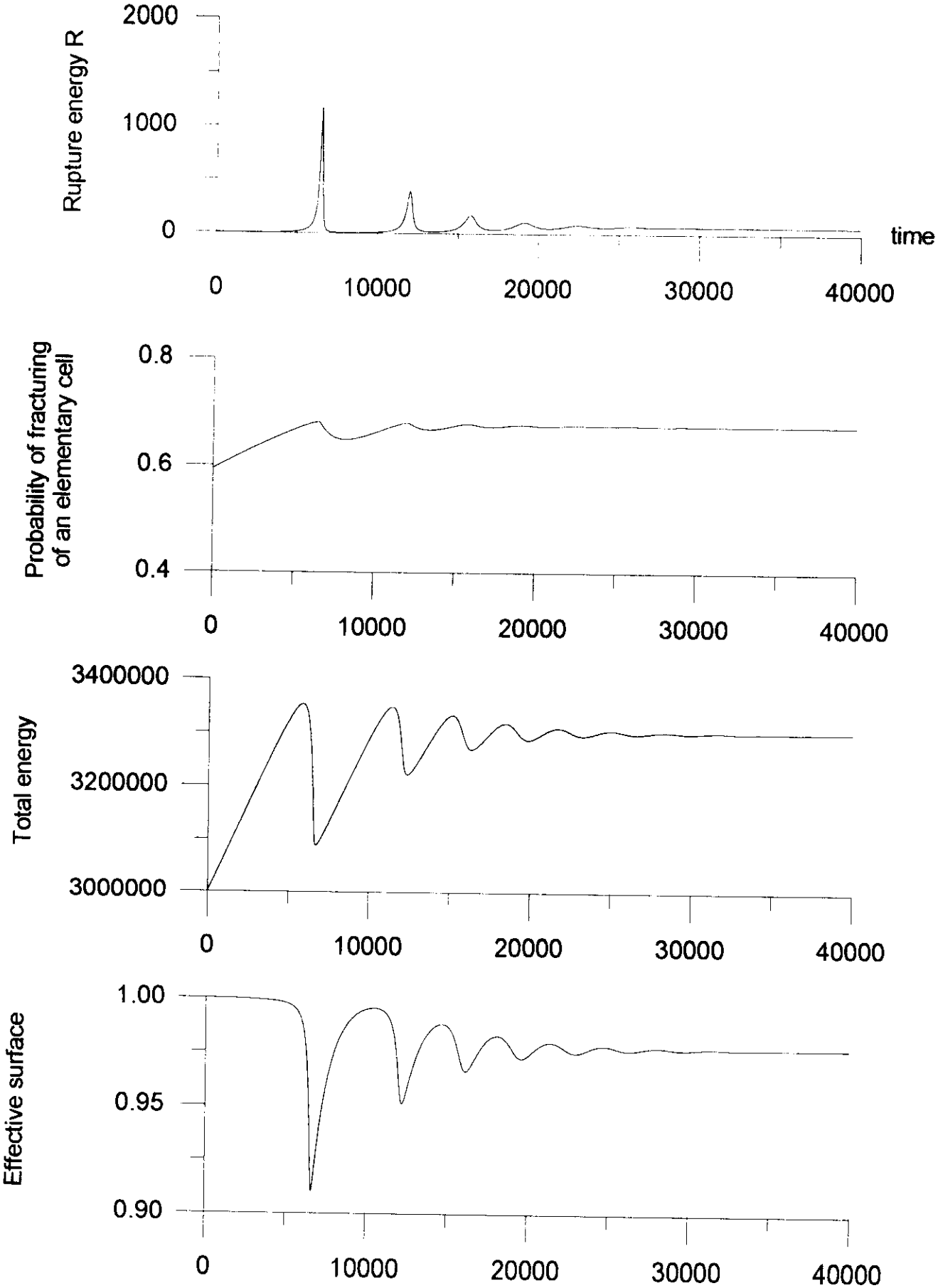
Rupture energy R
2000
1000
0
time
0
10000
20000
30000
40000
Probability of fracturing of an elementary cell
0.8
0.6
0.4
0
10000
20000
30000
40000
Total energy
3400000
3200000
3000000
0
10000
20000
30000
40000
Effective surface
1.00
0.95
0.90
0
10000
20000
30000
40000

Fig. 9a

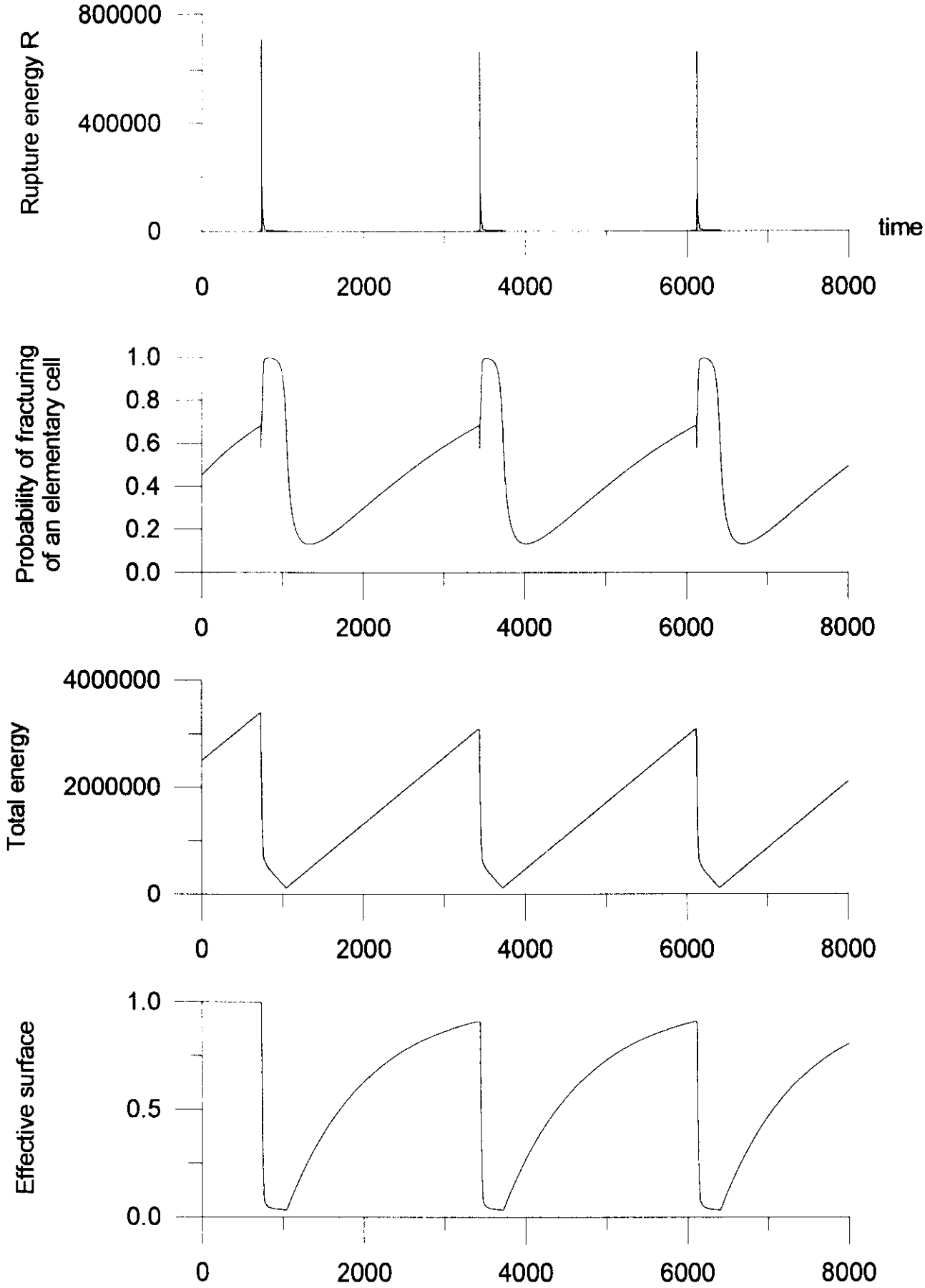
Rupture energy R
800000
400000
0
time
0
2000
4000
6000
8000
Probability of fracturing of an elementary cell
1.0
0.8
0.6
0.4
0.2
0.0
0
2000
4000
6000
8000
Total energy
4000000
2000000
0
0
2000
4000
6000
8000
Effective surface
1.0
0.5
0.0
0
2000
4000
6000
8000

Fig. 9b

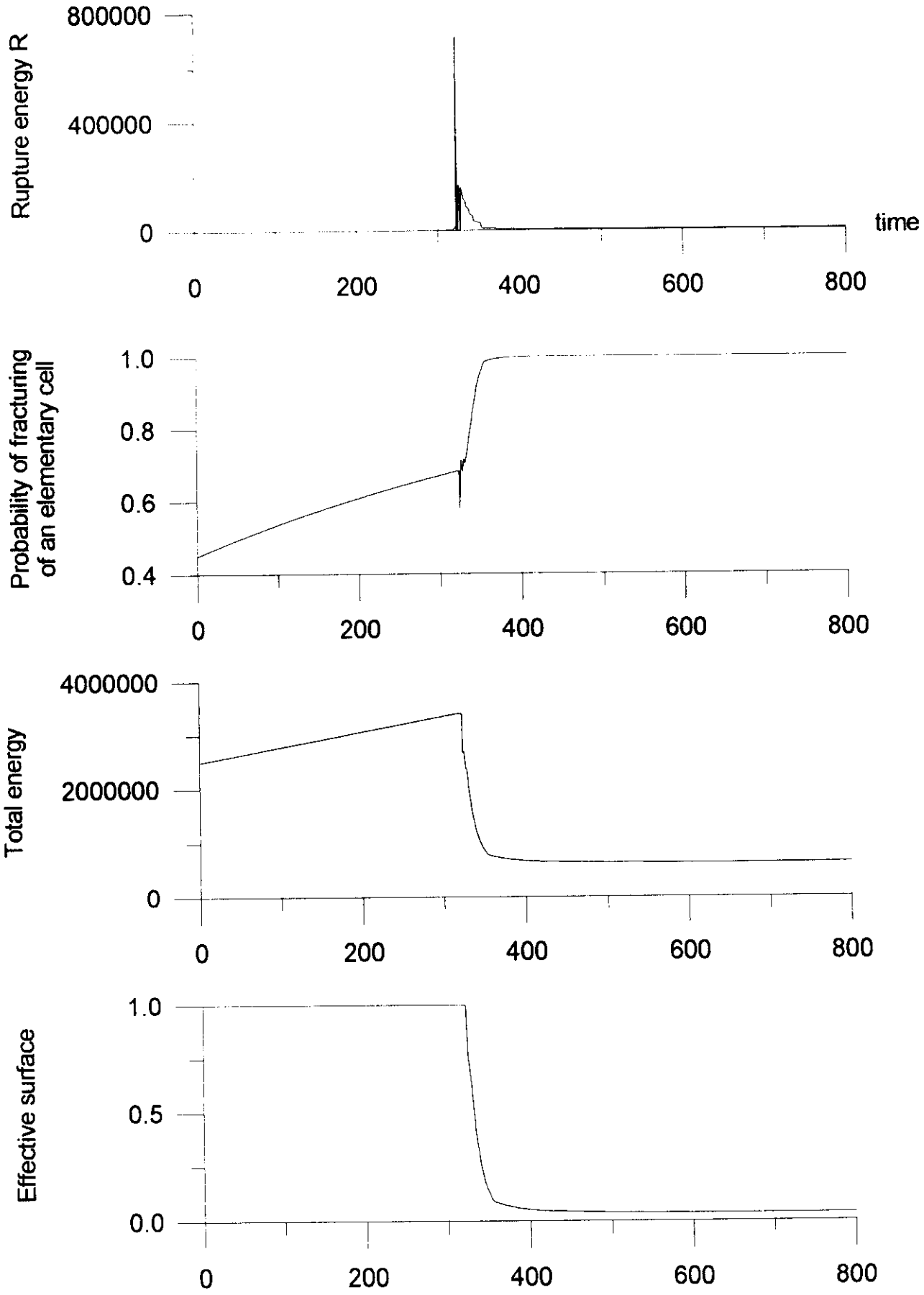
Rupture energy R
800000
400000
0
time
0
200
400
600
800
Probability of fracturing of an elementary cell
1.0
0.8
0.6
0.4
0
200
400
600
800
Total energy
4000000
2000000
0
0
200
400
600
800
Effective surface
1.0
0.5
0.0
0
200
400
600
800

Fig. 9c

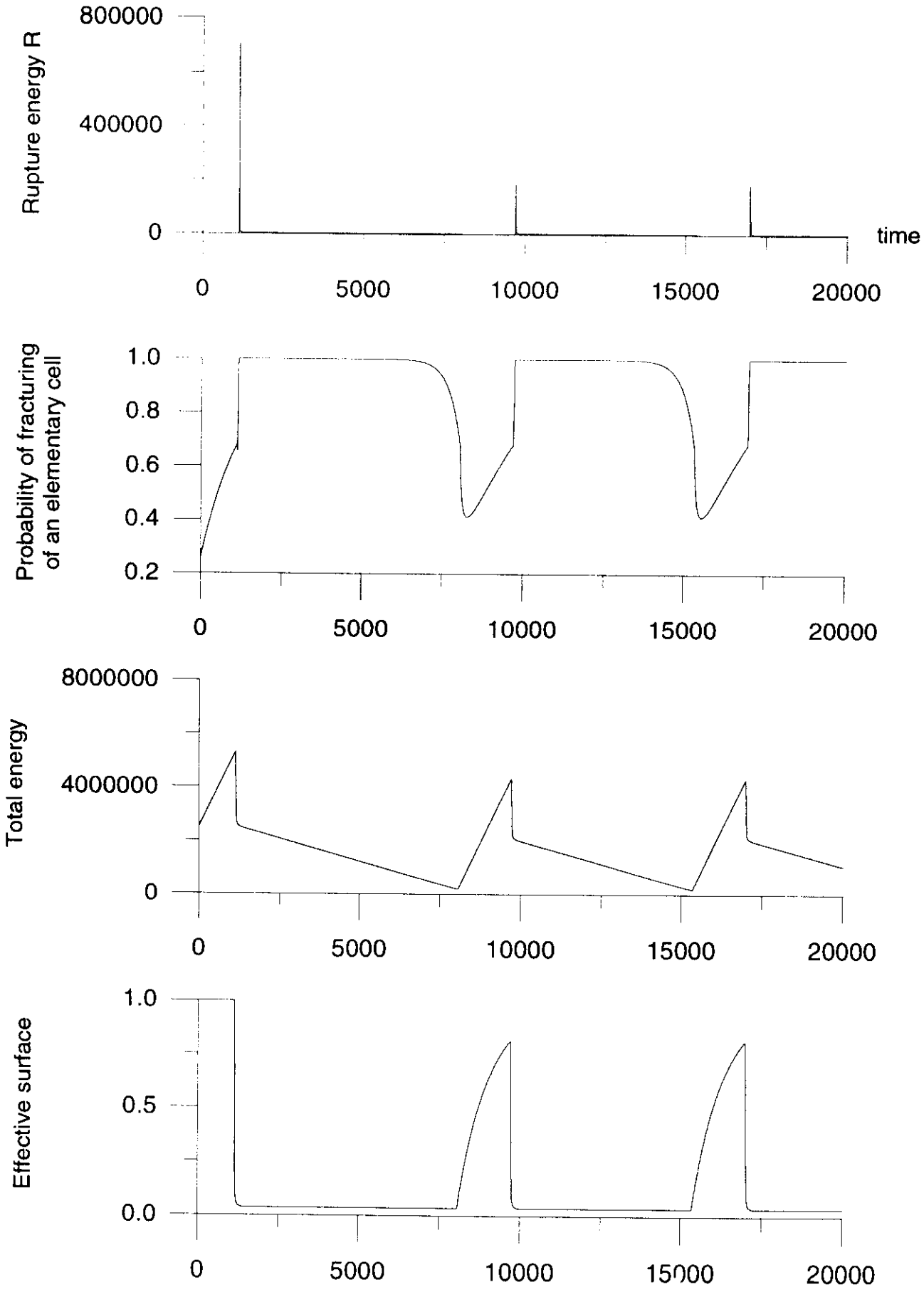
Rupture energy R
800000
400000
0
time
0
5000
10000
15000
20000
Probability of fracturing of an elementary cell
1.0
0.8
0.6
0.4
0.2
0
5000
10000
15000
20000
Total energy
8000000
4000000
0
0
5000
10000
15000
20000
Effective surface
1.0
0.5
0.0
0
5000
10000
15000
20000

Fig. 9d

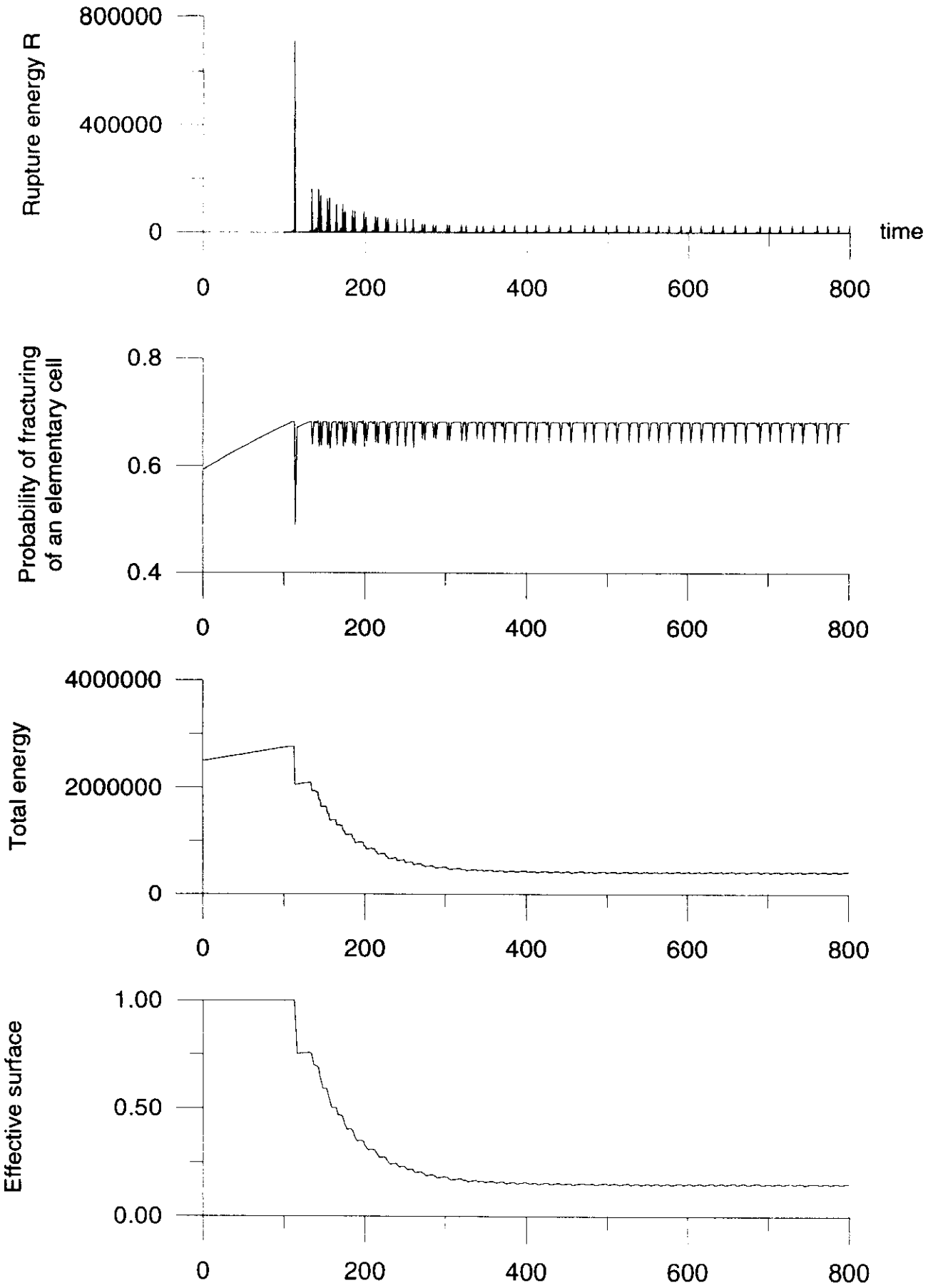
Rupture energy R
800000
400000
0
time
0
200
400
600
800
Probability of fracturing of an elementary cell
0.8
0.6
0.4
0
200
400
600
800
Total energy
4000000
2000000
0
0
200
400
600
800
Effective surface
1.00
0.50
0.00
0
200
400
600
800

Fig. 9e

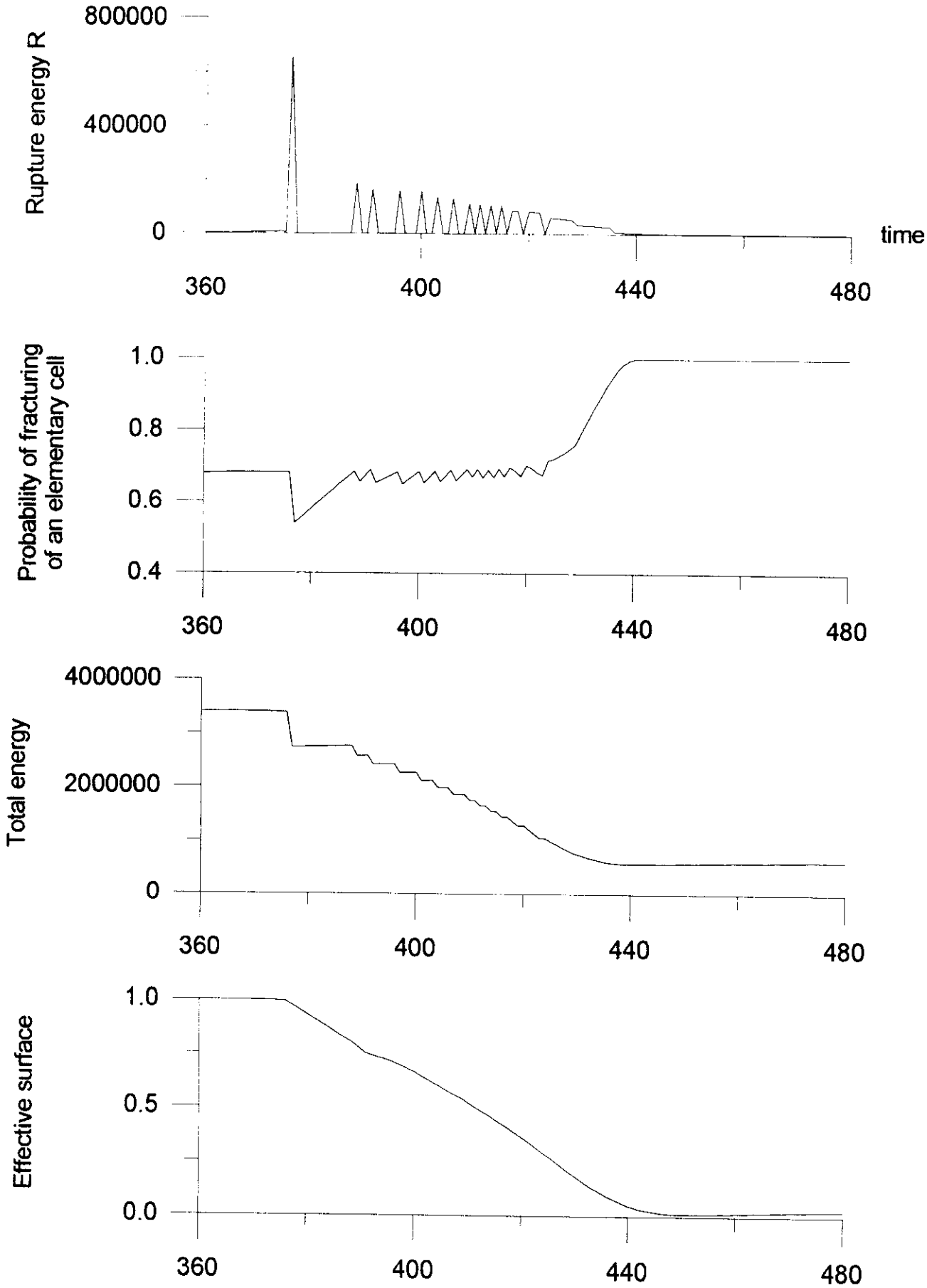
Rupture energy R
800000
400000
0
time
360
400
440
480
Probability of fracturing of an elementary cell
1.0
0.8
0.6
0.4
360
400
440
480
Total energy
4000000
2000000
0
360
400
440
480
Effective surface
1.0
0.5
0.0
360
400
440
480

Fig. 9f

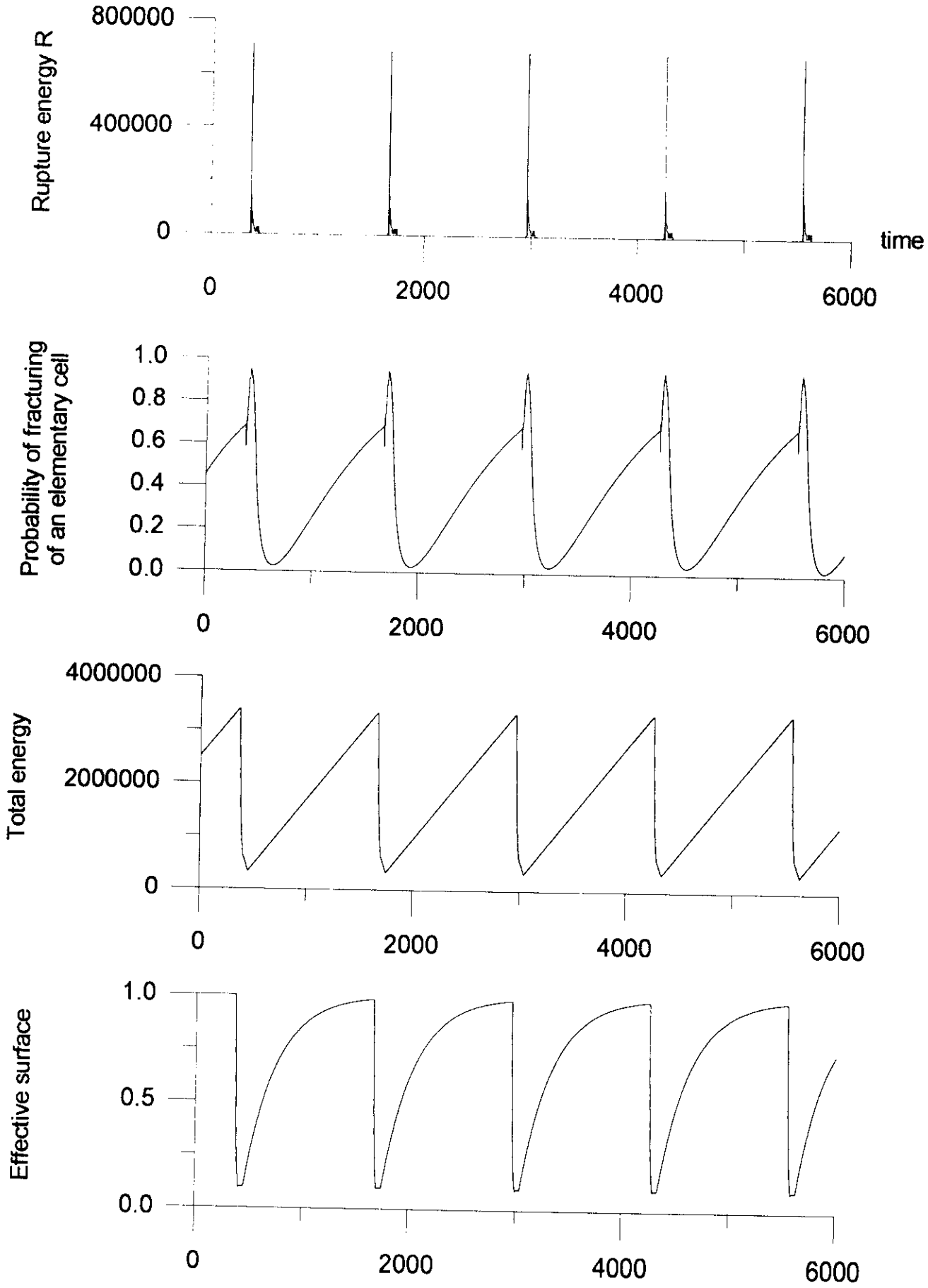
Rupture energy R
800000
400000
0
time
0
2000
4000
6000
Probability of fracturing of an elementary cell
1.0
0.8
0.6
0.4
0.2
0.0
0
2000
4000
6000
Total energy
4000000
2000000
0
0
2000
4000
6000
Effective surface
1.0
0.5
0.0
0
2000
4000
6000

Fig. 9g

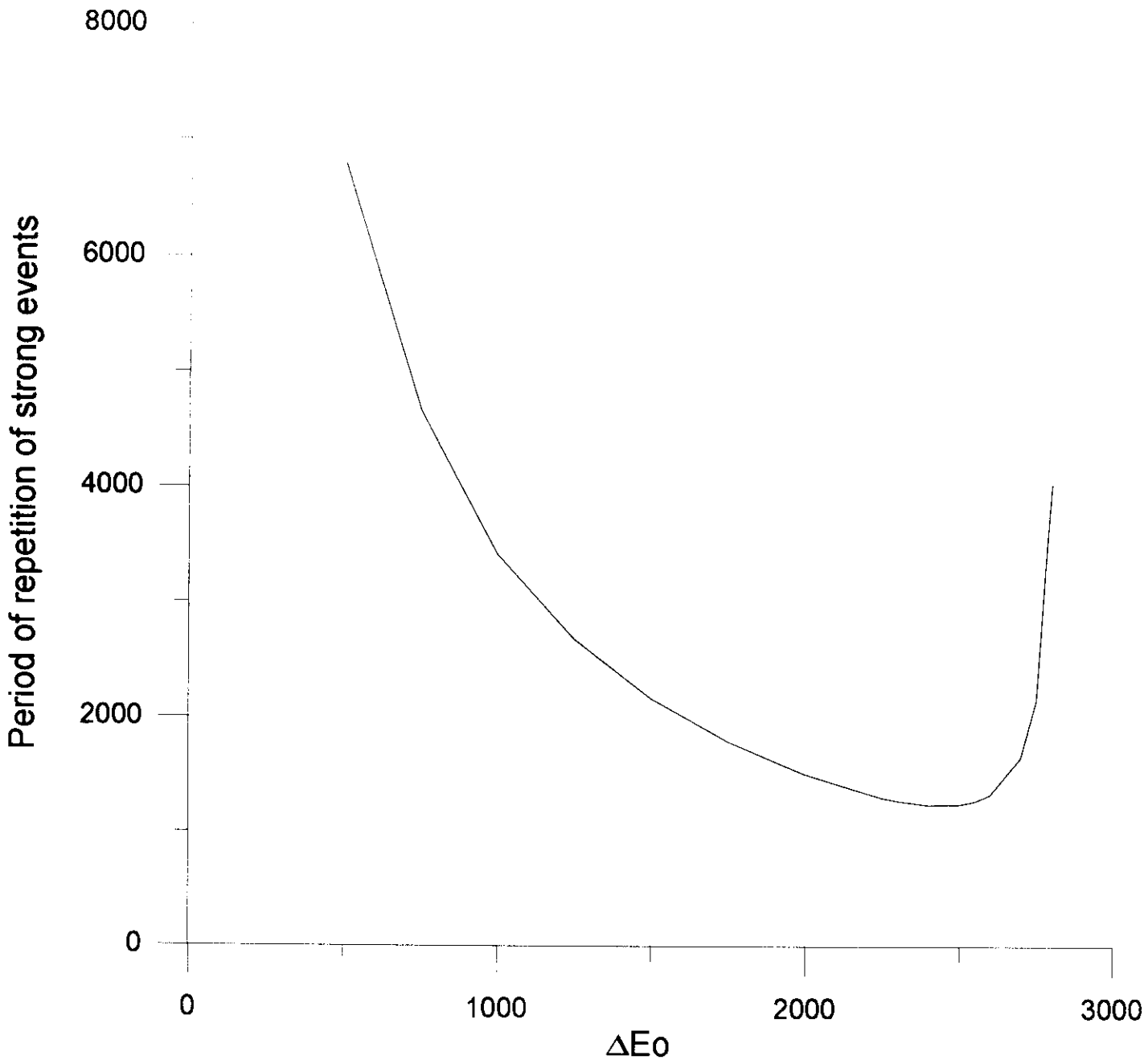
8000
6000
4000
2000
0
Period of repetition of strong events
0
1000
2000
3000
ΔEo

Fig. 10

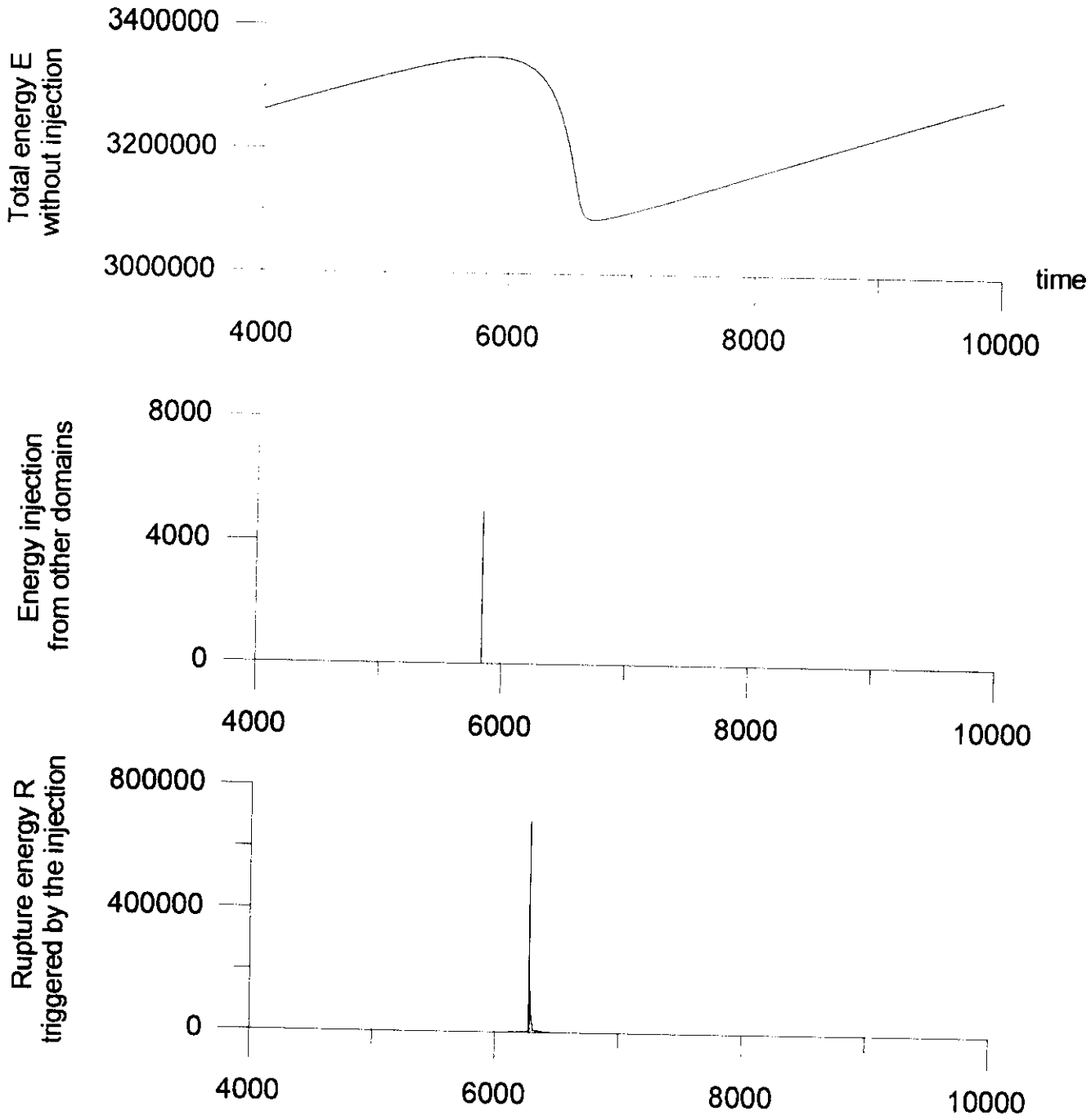
Total energy E without injection
3400000
3200000
3000000
time
4000
6000
8000
10000
Energy injection from other domains
8000
4000
0
4000
6000
8000
10000
Rupture energy R triggered by the injection
800000
400000
0
4000
6000
8000
10000

Fig. 11

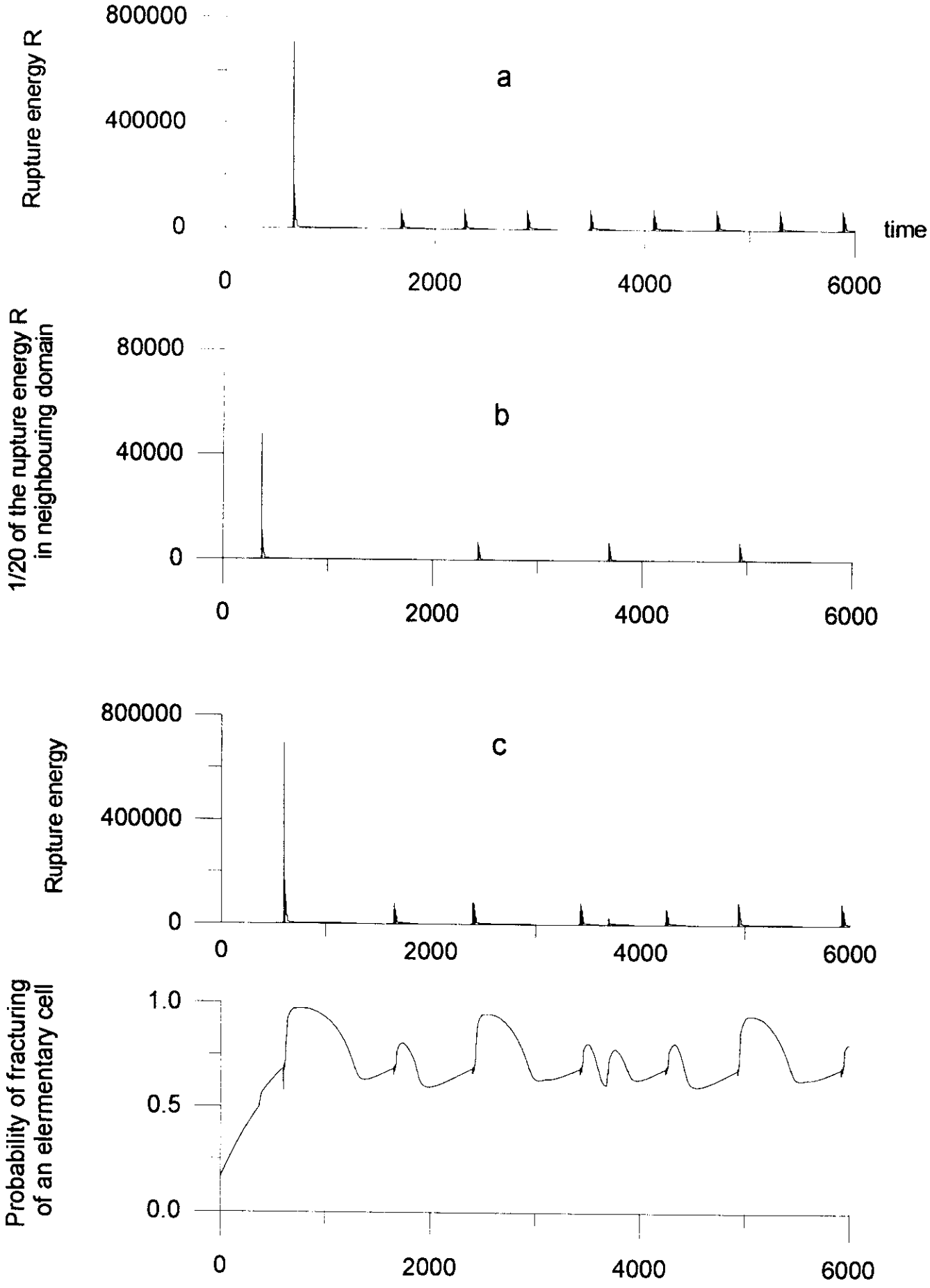
800000
400000
0
Rupture energy R
a
time
0
2000
4000
6000
80000
40000
0
1/20 of the rupture energy R
in neighbouring domain
b
0
2000
4000
6000
800000
400000
0
Rupture energy
c
0
2000
4000
6000
1.0
0.5
0.0
Probability of fracturing
of an elermentary cell
0
2000
4000
6000

Fig. 12

Hierarchical model of seismicity: scaling and predictability

E. M. Blanter, M. G. Shnirman, J. L. Le Mouël

Abstract

One considers the problem of the prediction of strong events in a hierarchical model of blocks moving in two directions. The model exhibits a linear magnitude-frequency relationship with variations in time of the local slope, a behavior which is referred to as dynamic self-organized criticality. An algorithm of prediction is based on this variation of the local slope of the magnitude-frequency relationship. A wide range of predictability is observed when varying the parameters of the model. The relationship between the predictability of synthetic catalogs and some of the parameters of the model is investigated.

1 Introduction

Following the early approach of [Allègre et al, 1982], several recent developments have been published which use the renormalization group or scaling laws techniques to the study of earthquakes genesis [Allègre and Le Mouël, 1994; Allègre et al., 1995; Blanter et al.1996]. For example, a hierarchical system of blocks moving in two orthogonal directions was considered in a previous work. This model accounts for a lot of basic properties of observed seismicity, such as the Gutenberg-Richter law, the foreshock activity, the Omori law for aftershocks, and the seismic cycle.

An important feature of a complex system is the predictability of its behavior. For real seismicity the problem of predictability can be reduced to the predictability of strong earthquakes in time and/or space [Molchan, 1991]. The problem of predictability has already been considered for a few models having properties similar to the properties of real seismicity [Shaw et al,1992; Pepke and Carlson,1994; Narkunskaya and Shnirman, 1994]. In the

present work the problem of predicting strong events in synthetic catalogs is approached. The synthetic catalogs of events are generated by a hierarchical model of blocks with two directions of movement, similar to the model described in our previous work [Blanter et al., 1996], although simpler.

The magnitude-frequency relationship describing the distribution of events in synthetic catalogs generated by the model appears to be similar to the Gutenberg-Richter law for real seismicity:

$$\ln N(E) = A - b \ln E \tag{1}$$

The linear behavior of the magnitude-frequency relationship in a large domain of the model parameters is characteristic of self-organized criticality [Bak et al, 1988; Blanter and Shnirman, 1996; Barriere and Turcotte, 1994]. In the model described in [Blanter et al.1996] the slope of the magnitude-frequency relationship varies with time and reflects the activity of events. This behavior was referred to in [Blanter et al.1996] as "dynamic self-organized criticality". Temporal variations of seismic activity are currently used in several algorithms of earthquake prediction [Keilis-Borok and Rotwain, 1990; Keilis-Borok and Kossobokov, 1990; Narkunskaya and Shnirman, 1994]; the variations of slope and form of the Gutenberg-Richter law may reflect the variations of seismic activity preceding a strong earthquake [Narkunskaya and Shnirman, 1994]. The present work shows that the strong events of the artificial catalogs are preceded by a decreasing of the absolute value of the slope of the magnitude-frequency relationship. Therefore the dynamic self-organized criticality allows the prediction of strong events through the examination of the slope of the magnitude-frequency relationship observed in the time interval preceding the event.

The quality of the prediction in the model is estimated using the (n, τ) diagrams proposed in [Molchan, 1991]. It comes out that the quality of the prediction depends on the model parameters: in some cases it may be much better than in the case of real seismicity [Keilis-Borok and Rotwain, 1990; Keilis-Borok and Kossobokov,1990; Narkunskaya and Shnirman, 1994], in other ones the prediction is completely random. For some values of the parameters of the model, the predictability of the events corresponding to the two orthogonal directions of motion may be rather different. The difference in predictability for different types of catalogs of events could be important to help understand why algorithms of prediction fail in some seismic regions [Rotwain, personal communication].

The next section contains the description of the considered model, and its behavior is described in section 3. The present model is a new version of our previous one [Blanter et al.1996], with some modifications. As the former model was rather complicated, we reduce here the number of parameters. This reduction simplifies the equations governing the appearance of moving blocks and the energy dynamics. But some features of the model behavior, such as the Omori law, are lost due to this reduction. Fluctuations are introduced in the model by replacing the mean values of the intervening functionals by a random realization of events. The definition of a critical configuration, previously adopted as "3 from 4", is now changed in a "2 from 4", which makes easier the appearing of new motions in the system.

The general problem of prediction is discussed in section 4. In the same section concrete rules for the declaration of alarms and for the comparison of predictions are given. Results of prediction applied to catalogs generated by the model for various values of the parameters are described in sections 5-6. The results and possible applications are discussed in section 7.

2 Model description

Let us consider a hierarchical system of blocks (Fig. 1). Four blocks of a given level l compose a block of the upper level $(l+1)$. The total number of blocks of $(l+1)$ level is four times less than the total number of blocks of l level. There is a single block at the highest level of the system. The area of a block at l level is four times less than at $(l+1)$ level.

There are four possible states for each block of the system. A block may be motionless, it may move along the direction e_1, move along the orthogonal direction e_2, or move simultaneously along the two directions e_1 and e_2. We consider motions of blocks which are small in comparison with their linear sizes, therefore assuming that the spatial coordinates of the blocks remain unchanged. A motion of a block of lth level initiated at time t along the direction e_i is referred to as an event of lth level of ith direction. Motions appear on the first level of the system and are sequentially transferred to the upper levels during one time unit. The appearance of motions at the initial level along the direction e_i is determined by a functional $E_i(t)$ whose dynamics is similar to an energy dynamics with a constant input ΔE_i and a dissipation term depending on all the events which appeared in the system at the previous time moment $(t-1)$. A block of lth level which does not

move along the direction e_i at time t may start moving along this direction at time $(t+1)$ with the appearance probability $\alpha_i(l,t)$. It is assumed that the appearance probability $\alpha_i(l,t)$ at level l is determined by the density of new critical configurations of blocks moving along the direction e_i which appear at the same time t at the lower level $(l-1)$. A configuration of blocks in a group of four elements is called critical for the direction e_i if it consists of more than one block moving along this direction. The critical configuration is called new for time t if there is one or more blocks which started moving along e_i at time t and if there was less than two blocks moving along this direction at time $(t-1)$. Thus the appearance probabilities $\alpha_i(l,t)$ are completely determined by the state of the previous level $(l-1)$ at the same time t.

Each block of lth level moving along the direction e_i at time t may have stopped this motion along this direction at time $(t+1)$ with the probability $\beta_i(l,t)$ (damping probability). Thus the motion of the blocks results from two opposite processes: the appearance of new moving blocks and the stopping of old moving blocks.

2.1 Number of events

The number of blocks of l-th level moving in the direction e_i (i=1,2) at time t can be expressed as follows:

$$N_i(l,t) = N_i^{new}(l,t) + N_i^{old}(l,t) \tag{2}$$

where $N_i^{new}(l,t)$ is the number of blocks which started moving during time interval $(t-1,t)$, and $N_i^{old}(l,t)$ is the number of blocks which moved at time $t-1$ and have not stopped. New motions of blocks are referred to as events (model analogues to earthquakes). In the present paper we will investigate the predictability of synthetic catalogs of such events as given by the model.

Each motionless block on level l may start moving in the direction e_i during the time interval $(t,t+1)$ with the probability $\alpha_i(l,t)$, which is called the appearance probability. Let us denote the total number of blocks of level l as $N(l)$, then $N(l) = 4^{L-l}$, where L denotes the total number of levels in the system. To obtain the number of events of level l at time $t+1$, we realize $N(l) - N_i(l,t)$ binomial random values ξ_n which are equal to unity with the probability $\alpha_i(l,t)$ and equal to zero with the probability $1-\alpha_i(l,t)$. Summing the random values we obtain the number of new events at time

$(t+1)$:

$$N_i^{new}(l, t+1) = \sum_n \xi_n \tag{3}$$

A block of level l moving along the direction e_i at time t may have stopped at time $t+1$ with a probability $\beta_i(l,t)$ (damping probability). To obtain the number of blocks which have not stopped at time $t+1$ we take the sum of $N_i(l,t)$ binomial random values ζ_n (the parameter of the distribution being $(1-\beta_i(l,t))$):

$$N_i^{old}(l, t+1) = \sum_n \zeta_n \tag{4}$$

In the present paper we simulate the number of events at each time moment and for each level and direction in contrast to what was done in the previous one [Blanter et al, 1996], where we calculated only the mean values of the densities of moving blocks. This direct simulation allows to introduce fluctuations that may be significant to give a chaotic temporal distribution of events, similar to the distribution of earthquakes. This is important for the problem of prediction.

2.2 Energy relationships

The density of events of level l along the direction e_i at time t is defined as follows:

$$p_i^e(l,t) = \frac{N_i^{new}(l,t)}{4^{L-l}} \tag{5}$$

Let us define the energy dissipation function for events of i-th direction at time t as follows:

$$R_i(t) = \sum_{l=1}^{L} q^l p_i^e(l,t) \tag{6}$$

As in paper [Blanter et al, 1996] we introduce two functionals, called the energy functionals, which govern the appearance probabilities at the first level. The temporal evolution of these energy functionals is as follows:

$$E_1(t+1) = E_1(t) \exp\left(\frac{\Delta E_1 - \lambda_{11} R_1(t)}{E_1(t)}\right) \cdot \exp\left(\frac{-\lambda_{12} R_2(t)}{E_2(t)}\right) \tag{7}$$

$$E_2(t+1) = E_2(t) \exp\left(\frac{\Delta E_2 - \lambda_{21} R_2(t)}{E_2(t)}\right) \cdot \exp\left(\frac{-\lambda_{22} R_1(t)}{E_1(t)}\right) \tag{8}$$

Expressions (7) and (8) mean that the evolution of the energy functional $E_i(t+1)$ is governed by the constant energy input rate ΔE_i and the energy dissipation functions $R_i(t)$. According to expression (6) the energy functionals depend on all the events which occurred in the system at the previous time moment t. Coefficient λ_{ij} adjusts the influence on E_i of the dissipation along the j-th direction. A negative value of λ_{ij} means a positive contribution of $R_j(t)$ to E_i.

The appearance probabilities at the first level of the system are defined as follows:

$$\alpha_i^1(t) = 1 - \exp(-kE_i(t)), \quad i = 1, 2 \tag{9}$$

2.3 Rule of transmission of the motion to upper levels

A block of level $l+1$ starts moving along direction i when a new critical configuration of blocks moving in this direction appears at the previous level l. In our previous investigations [Blanter et al, 1996] we formulated the following conditions to obtain a new critical configuration of level l for i-th direction at time $t+1$:

1. Two or less blocks were moving along the direction e_i in a group of four blocks of level l at time t.
2. One or more new blocks of the group begin to move at time $t+1$.
3. As a result, three or more blocks of the group move along the direction e_i at time $t+1$.

We claimed [Blanter et al, 1996] that such a definition of the critical configuration produces a model more stable than the lithosphere. Therefore we change here the condition 3 and require two or more blocks of the group moving at time $t+1$. The appearance probabilities $\alpha_i(l+1)$ are then expressed by the following conditional probability:

$$\alpha_i(l+1,t) = P\{0\}\frac{6\alpha_i^2(l,t)(1-\alpha_i(l,t)^2) + 4\alpha_i^3(l,t)(1-\alpha_i(l,t)) + \alpha_i^4(l,t)}{P\{0\}+4P\{1\}+6P\{2\}} +$$

$$+4P\{1\}\frac{3\alpha_i(l,t)(1-\alpha_i(l,t))^2(1-\beta_i(l,t)) + 3\alpha_i^2(1-\alpha_i(n,t)) + \alpha_i^3(l,t)}{P\{0\}+4P\{1\}+6P\{2\}} +$$

$$+6P\{2\}(\frac{(2\alpha_i(l,t)(1-\alpha_i(l,t))(1-\beta_i(l,t)^2) + \alpha_i^2(l,t)}{P\{0\}+4P\{1\}+6P\{2\}} \tag{10}$$

$P\{k\}$ $(0 \leq k \leq 4)$ is the probability for k blocks of level l to move along i-th direction in the group of 4 blocks composing a block of the upper level $l+1$. Probabilities $P\{k\}$ can be easily expressed from densities of moving blocks $p_i(l,t)$:

$$P\{0\} = (1-p_i(l,t))^4; \qquad P\{1\} = p_i(l,t)(1-p_i(l,t))^3;$$

$$P\{2\} = p_i^2(l,t)(1-p_i(l,t))^2; \qquad P\{3\} = p_i^3(l,t)(1-p_i(l,t));$$

$$P\{4\} = p_i^4(l,t).$$

2.4 The damping probability

The probability of damping results from the friction between the blocks. The friction between a block moving along e_1 and its neighbors is enhanced by a motion along e_2 through the corresponding increase of pressure. The friction damping the motion along e_1 is also likely to grow with the motion density along this same direction (due for example to asperities in the faults). Then the damping probability β_1 will be supposed to depend on the densities of events (new motions) p_2^e, p_1^e, and also on the older motions of blocks at the same level. We assume that the contributions of events of older motions are different. The difference is introduced with the help of coefficient γ. Furthermore, the damping probabilities will be supposed to have scaling properties: all of them contain an exponential function of level; it means that the lifetime of motions of higher levels is larger than that of motions of lower levels for a same density of motions. The probability of damping at the l-th level is thus defined as follows:

$$\begin{aligned}\beta_1(l,t) = (c_0 + (c_1 - c_0)(p_2^e(l,t) + \gamma(p_2(l,t) - p_2^e(l,t)) + \\ +(c_2 - c_1)(p_1^e(l,t) + \gamma(p_1(l,t) - p_1^e(l,t)))\delta^l \qquad (11)\\ \beta_2(l,t) = (c_0 + (c_1 - c_0)(p_1^e(l,t) + \gamma(p_1(l,t) - p_1^e(l,t)) + \\ +(c_2 - c_1)(p_2^e(l,t) + \gamma(p_2(l,t) - p_2^e(l,t)))\delta^l \qquad (12)\end{aligned}$$

The choice of parameters c_i allows to vary the various contributions to the probability of damping. The condition $0 \leq c_0 \leq c_1 \leq c_2 \leq 1$ is to be satisfied, δ is a scaling parameter $0 \leq \delta \leq 1$.

3 General behavior of the model

3.1 Temporal distribution of events

The present paper is devoted to the problem of prediction. Therefore the most important properties of the model are those related to the distribution in time of events of higher levels. It is possible to obtain a regular distribution of strong events (Fig. 2a) or a chaotic distribution of these events similar to the distribution of real earthquakes, which was not achieved in the previous model [Blanter et al, 1996] (Fig. 2b). The chaotic behavior is related to the fluctuations introduced in the present model by the direct simulation of the number of events.

3.2 The magnitude-frequency relationship

In seismology the magnitude M serves as a measure of the earthquake volume; it is connected with the area of the nucleation zone S (Utsu and Seki, 1954)]:

$$\lg S \approx M + const \tag{13}$$

We assume that the area of each block of level l is equal to $C4^l$. Therefore the magnitude of the events of level l of the system may be defined as follows:

$$M_l = l \lg 4 \tag{14}$$

To compare the synthetic distribution of events with the distribution of real earthquakes, we have generated a synthetic catalog of events of higher levels; it includes the occurrence time and the magnitude of these events.

In log/log plot the magnitude-frequency relationship for events occurring during a long enough interval $(t, t+T)$ is approximately linear for different model catalogs displaying either a chaotic or a regular distribution of events (Fig. 3).

The magnitude-frequency relationships calculated for temporal intervals $(t, t+\tau)$ characterized by different activity display linear trends with variable slopes. This kind of behavior was called dynamic self-organized criticality in our previous paper. The value of the slope is smaller in periods of low activity and larger in periods containing a high density of strong events (Fig. 4). Furthermore, the slope of the magnitude-frequency relationship increases before the occurrence of events of the highest level and may provide a good precursor of strong events (as will be now examined).

4 The problem of prediction

The simplest way to enounce the problem of earthquakes prediction is: taking into account the information about seismicity available for the time interval $(t-\Delta, t)$, can we announce that a strong event will take place or not at time $t+1$? Usually the prediction is based on one or more functionals, and the alarm is declared when the functionals reach some threshold value. Events appearing during the alarm period are referred to as successes, the other events as errors. A distinct rule governs the termination of the declared alarm.

Let us take the slope of the magnitude-frequency relationship as the functional of prediction. If the slope $b(t)$ calculated for the time interval $(t-\Delta, t)$ is larger than or equal to a threshold value η, then an alarm is declared for time $t+1$. If the slope is less than η, then there is no alarm for time $t+1$. The alarm times and the times of events of the highest level (as given by the model computation) are plotted on Fig.5.

4.1 The estimation of the quality of a prediction with the (n, τ) diagram

The quality of an algorithm of earthquake prediction may be estimated using the (n, τ) diagram [Molchan, 1991]. Each prediction with fixed parameters of the algorithm corresponds to a point (n_0, τ_0) on the (n, τ) diagram, where n_0 is the percentage of unpredicted events and τ_0 is the ratio the time of alarms to the total time interval considered. A set of points (n_0, τ_0) for different values of the threshold value η (the other parameters of the model being kept inchanged) composes a curve of the (n, τ) diagram. For a random prediction the ratio of successes is approximately equal to the ratio of alarms, so the corresponding (n, τ) diagram is the straight line $n + \tau = 1$. A nontrivial prediction is possible if the (n, τ) diagram which corresponds to the considered algorithm of prediction is sufficiently below the straight line of random prediction (Fig. 6a).

Our rule for declaring and terminating on alarm depends on a single parameter, the threshold value η; the (n, τ) diagram is obtained by eliminating η. Such diagrams, illustrating the quality of the prediction of the strongest events ($l = 16$), for two types of synthetic catalogs, are showed on Fig. 6a. The dashed line ($n + \tau = 1$) corresponds to the random prediction. Consider two predictions with characteristic values n_1, τ_1 and n_2, τ_2; if $n_1 < n_2$ and

$\tau_1 < \tau_2$, the first prediction is clearly better than the second one. It is thus possible to compare two predictions by comparing their (n, τ) diagrams; if one diagram is below the other one, the first prediction is better than the second one. For example, as illustrated by Fig. 6a, considering catalogs generated by our model, the prediction for a "regular catalog" is much better than the prediction for a chaotic one; and the prediction for both of them is better than a random prediction.

4.2 The choice of threshold of prediction η

When predictability of events in a real system is investigated, the threshold of prediction is selected such as to minimize a loss function. If the loss function is unknown, the minimax strategy is often used [Keilis-Borok and Rotwain, 1990; Keilis-Borok and Kossobokov,1990]. In the present investigation we choose the threshold value in such a way as to minimize the total prediction error defined as:

$$\phi(\eta) = n(\eta) + \tau(\eta) \tag{15}$$

The total error function, $\phi(\eta)$, plotted on Fig. 6b, presents a clear minimum for the best value of the threshold η. The total error $\phi(\eta)$ corresponding to the regular catalog is below the total error for the chaotic catalog. In other words the prediction for the regular catalog is better than the prediction for the chaotic catalog; and the functions $\phi(\eta)$ for both catalogs are smaller than unity (the value corresponding to the random prediction).

5 "Predictable" and "unpredictable" catalogs

The two examples of catalogs we discussed above demonstrate that the predictability of strong events depends on the catalog, for a given algorithm of prediction (Fig. 6). Let us look for what the predictability depends on. We draw a number of realizations of a catalog, first in the regular, then in the chaotic case (with fixed parameters in each case); we compute the $(n(\eta), \tau(\eta))$ values for each realization, then the average (n, τ) diagram for the set of realizations, and two more curves characterizing the variability of the estimates (Fig. 7). One can see that the variability of the (n, τ) diagram with the different realizations of a same process (fixed parameters of the model) is not large. The graphs of the total error $\phi(\eta)$ show the same stability (Fig. 8).

Thus the predictability of strong events in synthetic catalogs is governed by the inner parameters of the model.

By varying these parameters it is possible to obtain a total error of prediction $o(\eta) < 0.01$ for the best values of the threshold η. This quality of prediction is much better than any estimation obtained in prediction of real seismicity [Keilis-Borok and Rotwain, 1990; Keilis-Borok and Kossobokov,1990]. But for other parameters of the model the prediction for our synthetic catalogs may be completely random. A big variation of predictability may be achieved by changing only the damping parameters (see Fig. 6). The predictability of synthetic catalogs is connected with the temporal distribution of great events; both catalogs of Fig. 2 have the same number of events of the 16th level, but the distribution in time of these events is less chaotic on Fig. 2a than on Fig. 2b. The regular catalog is more predictable than the chaotic one. The chaotic behavior of the "unpredictable" catalog is also reflected in the behavior of the local slope $b(t)$ of the magnitude-frequency relationship (Fig. 4b); the behavior of $b(t)$ for the "predictable" catalog is more regular than for the "unpredictable" one (Fig. 4a).

5.1 Relationship between predictability and energy rate

In [Allègre et al, 1995], in the case of an unidirectional model, the onset of seismicity was studied in function of the energy input rate ΔE (starting from an unloaded state). When ΔE was small, no strong event occurred; for large values of ΔE, strong events occurred without any precursor; for intermediate values of ΔE, a strong event was preceded by precursors. Let us look at the influence of ΔE in the present model (2-D and in which we consider an indefinite sequence of events rather than the onset of a single phase of seismicity). To have a single parameter ΔE instead of two, we fix the ratio $\Delta E_2/\Delta E_1 = 5$. Then the rate $\Delta E = \Delta E_1$ is varied from 0.5 to 50. When the energy rate grows from $\Delta E = 10$ to $\Delta E = 50$ the predictability monotonically decreases; the best threshold of prediction remains unchanged (Fig. 9a). When the energy rate ΔE decreases from 5 to 0.5 the predictability of the model falls down and the best threshold of prediction presents a small decreasing (Fig. 9b). For values of the energy rate going from 5 to 10 there is a clear variation of the best threshold without any significant change of the quality of the prediction (Fig. 9a).

6 Different predictability of the two kinds of events

There are two kinds of events in our model: events of the first kind correspond to the direction e_1, events of the second kind correspond to the direction e_2. Let us denote n_1 the ratio of unpredicted events of the first kind and n_2 the ratio of unpredicted events of the second kind. If τ is the ratio of alarms, defined as above, we define the total error of prediction for events of ith kind as:

$$\phi_i(\eta) = n_i(\eta) + \tau(\eta) \tag{16}$$

For all catalogs considered above the total error of prediction is the same for both kinds of events:

$$\phi_1(\eta) \approx \phi_2(\eta) \approx \phi(\eta) \tag{17}$$

But it is possible to choose the parameters of the model such that the predictability be different for the two kinds of events (Fig. 10). In this example the total error of prediction for the first kind of events is better than the total error for the second kind, or for all the events. The best threshold value η_2 for the second kind of events is less than the best value η_1 for the first kind. Thus a prediction performed with the threshold value η_1 will be successful for the events of the first kind but will fail to predict the events of the second kind. Let us consider the magnitude-frequency relationships calculated separately for the two kinds of events on the whole time interval $T = (0 - 40000)$ (Fig.11). The curve 1 corresponding to the first kind of events is situated below the curve 2 and presents an upward bend; the curve 2 on the contrary presents a weak bend downwards. Thus the upward bend of the global magnitude-frequency relationship is due to the events corresponding to the direction with the best predictability.

Calculations show that the relation between the predictability and the bend of the magnitude-frequency curve remains valid for all realizations of the model (for all sets of parameters). When the energy rate ΔE increases from 1 to 10 (all the other parameters been kept fixed), the magnitude-frequency relationship for both directions keeps an upward bend, and the difference in predictability for the two kinds of events decreases. When the energy rate ΔE is equal to 1, the second curve presents a downward bend (Fig.11) and there is a difference in predictability for the two directions. All the simulations have been made with all parameters of the system fixed, except the energy rate.

7 Conclusions and discussion

We have obtained the result that there is a big variability in the predictability of the model catalogs, which depends on the inner parameters of the model, such as the damping parameters and the energy rate. Investigations on predictability of real seismicity show that some algorithms of prediction appear to be successful in some seismic regions, where the total error of (retrospective) prediction would be near 0.4 [Keilis-Borok and Rotwain, 1990]. But, applied to some other regions, such as subduction zones, the same algorithm gives $\varphi > 1$ [Rotwain, personal communication]. This phenomenon may be connected with a difference between the inner parameters of the seismic process in "predictable" and "unpredictable" regions. Investigation of the connection between the model parameters and the predictability of the corresponding catalogs may help to find similar relationships in real seismicity.

We have seen that for energy rates $0.5 < \Delta E < 50$ (Fig. 9a,b) the total error of prediction for the best threshold values is less then 0.76, which is close to the value 0.78 found for the total error of forward prediction in the case of real seismicity [Novikova and Rotwain, 1996]. Differences in the energy rate in real seismicity are not expected to exceed 1-1.5 orders of magnitude. So based on the present model, the existence of "unpredictable" seismic regions would seem to be connected with the damping conditions rather than with the value of the energy rate.

The difference of predictability for the two orthogonal kinds of events may be useful in understanding the nature of the unpredicted earthquakes for a given algorithm of prediction. It will be interesting to separate all earthquakes into predicted and unpredicted events, and to investigate the relationship between the predictability of each group and the main direction of motion for this group. If a relation is found, it will be possible to improve the algorithm of prediction by selecting the prediction thresholds separately for each group. The difference in predictability for the two kinds of events is reflected in the bend of the corresponding magnitude-frequency relationship calculated for the whole time span of simulation. But this criterion cannot be applied to synthetic catalogs corresponding to different parameters of the model: the regular and the chaotic catalogs represented on Fig. 2a,b both present upward bends in their magnitude-frequency curves (Fig. 3a,b), but have very different predictabilities (Fig. 6a,b).

Evidence of predictability for a wide set of parameters of the model is

the main result of the paper. The predictability of self-organized systems was previously considered in the paper of Pepke and Carlson [Pepke and Carlson, 1994]. It depends in most cases on the structure of the model; there are predictable models [Shaw et al, 1992], or unpredictable ones, such as the avalanche model of Bak [Bak and Tang, 1989]. No investigation of the variation of the predictability with the model parameters is made in [Shaw et al, 1992]; in the avalanche model [Bak and Tang, 1989], there are no parameters at all. No convincing variation of predictability was observed in the model of Olami et al. [Olami et al., 1992], and whether this model exhibits a self-organized criticality behavior has been debated [Socolar et al, 1991]. The present work shows that predictability may be a property of the parameters of the system, and not of its global structure.

We have also evidenced the connection existing between predictability and other properties of the distribution of events: the predictability of synthetic catalogs appears to be connected with the regularity of the temporal distribution of events; more regular catalogs are more predictable, more chaotic catalogs are less predictable. The difference of predictability of events along the two orthogonal directions is reflected in the bend of the magnitude-frequency relationship: an upward bend corresponds to the more predictable direction, a downward bend to the less predictable direction. Application of all these relationships to real seismicity may improve existing theories and help practical approaches to seismic prediction.

Acknowledgments The present work was completed in IPG Paris while E. Blanter and M. Shnirman had a visitory scientist grant in the frame of the IPGP/MITPAN cooperation agreement. The present work was also supported by Russian Foundation of Fundamental Research (project code 96-05-65710) and by NSF (project code EAR 94-23818). We acknowledge fruitful discussions with C. J. Allègre.

Fig.1 Hierarchical system of blocks. Four blocks of a given level compose a block of the upper level.

Fig.2 Temporal distribution of events in artificial catalogs. The plot shows events of levels 13 to 16. (a) – regular distribution of events; parameters of the model are: $L = 16$, $\Delta E_1 = 3.$, $\Delta E_2 = 15.$, $E_1(0) = E_2(0) = 4. \cdot 10^6$, $k = 1.2 \cdot 10^{-9}$, $q = 2$, $\lambda_{11} = 0.15$, $\lambda_{12} = -0.05$, $\lambda_{21} = 0.35$, $\lambda_{22} = -0.15$, $c_0 = 0.01$, $c_1 = 0.7$, $c_2 = 0.9$, $\gamma = 0.5$, $\delta = 0.9$; (b) – chaotic distribution of events; parameters of the model are: $L = 16$, $\Delta E_1 = 10.$, $\Delta E_2 = 50.$, $E_1(0) = E_2(0) = 3.2 \cdot 10^6$, $k = 1.2 \cdot 10^{-9}$, $q = 2$, $\lambda_{11} = 0.15$, $\lambda_{12} = -0.05$, $\lambda_{21} = 0.35$, $\lambda_{22} = -0.15$, $c_1 = 0.01$, $c_2 = 0.3$, $c_3 = 0.7$, $\gamma = 0.6$, $\delta = 0.8$.

Fig. 3 Magnitude-frequency relationship for regular (a) and chaotic (b) distributions of events on a time interval $\Delta T = 40000$. Parameters of the model are the same as for Fig. 2.

Fig. 4 Temporal evolution of the slope of the magnitude-frequency relationship for regular (a) and chaotic (b) distributions of events. The value of the slope increases in periods of high activity and decreases in periods of low activity (see Fig.2). Parameters of the model are the same as for Fig. 2.

Fig. 5 Alarm times and times of occurrence of strong events for regular (a) and chaotic (b) artificial catalogs. Alarm times are represented by rectangles below the horizontal axis, times of strong events are plotted above the axis. Parameters of the model are the same as for Fig. 2. The slope of the magnitude frequency relationship is calculated for levels 7 to 15, for each time interval $(t - \Delta, t)$, where $\Delta = 20$. The thresholds values used in the prediction are respectively $\eta = 1.1$ – (a), and $\eta = 1.$ –(b).

Fig. 6 Characteristic functions representing the quality of the prediction.

(a) — Average (n, τ) diagram for prediction of regular (1) and chaotic (2) catalogs. Model parameters are the same as for Fig. 2. The dashed line corresponds to a random prediction. The parameters of the prediction are the following: $\Delta = 20$, levels 7 to 15 used to calculate the slope functional. Events of 16th level are predicted.

(b) — Mean value of the total error of prediction ϕ vs the threshold value η for regular (1) and chaotic (2) catalogs. Model parameters are the same as for Fig. 2. The dashed line corresponds to a random prediction. Parameters of prediction are the same as for Fig. 6a.

Fig. 7 Variation of the (n, τ) diagram for different realizations of synthetic catalogs, keeping the parameters of the model constant. The solid line represents the mean value $\bar{n}(\tau)$ of the function, the dashed lines represent $\bar{n}(\tau) \pm \sigma$. (a) — regular catalog; the dashed straight line corresponds to a random prediction. (b) — chaotic catalog; the solid straight line corresponds to a random prediction. Parameters of the model are the same as for Fig. 2; parameters of prediction are the same as for Fig. 6.

Fig. 8 Variation of the total error of prediction for different realizations of synthetic catalogs, keeping the parameters of the model constant. The solid line represents the mean value $\bar{\phi}(\eta)$ of the function, the dashed lines represent $\bar{\phi}(\eta) \pm \sigma$. (a) — regular catalog; (b) — chaotic catalog. Parameters of the model are the same as for Fig. 2; parameters of prediction are the same as for Fig. 6.

Fig. 9 Total error of prediction $\phi(\eta)$ for different energy rates ΔE. Parameters of the model are the same as for Fig. 2a, except for energy rates: $\Delta E_2/\Delta E_1 = 5$, $\Delta E = \Delta E_1$. The prediction functional $b(t)$ is calculated for $\Delta = 20$.

(a) — $\Delta E \geq 5$. The total error grows (the predictability decreases) when the energy rate grows. The best threshold value is the same for curves (1-3): 1 — $\Delta E = 50$, 2 — $\Delta E = 30$, 3 — $\Delta E = 10$, 4 — $\Delta E = 5$. Events of 16th level are predicted, $b(t)$ is calculated for levels 7 to 15.

(b) — $\Delta E \leq 5$. The total error grows (the predictability decreases) when the energy rate decreases. The best threshold value increases with the energy rate ΔE. 1 — $\Delta E = 0.5$, 2 — $\Delta E = 1$, 3 — $\Delta E = 5$. For $\Delta E = 5$ events of 16th level are predicted and $b(t)$ is calculated for levels 7 to 15; for $\Delta E = 1$ and $\Delta E = 0.5$ events of levels 14 to 16 are predicted and $b(t)$ is calculated for levels from 7 to 13.

Fig. 10 Average of the total error of prediction for the two kinds of events. (1) — events corresponding to the direction e_1, (2) — events corre-

sponding to the direction e_2. Parameters of the model are: $L = 16$, $E_1(0) = E_2(0) = 2 \cdot 10^6$, $\Delta E_1 = 2$, $\Delta E_2 = 10$, $q = 2$, $k = 2.3 \cdot 10^{-9}$, $\lambda_{11} = 1$, $\lambda_{21} = 1.5$, $\lambda_{12} = \lambda_{22} = 0$, $c_0 = 0.01$, $c_1 = 0.7$, $c_2 = 0.9$, $\gamma = 0.6$, $\delta = 0.9$. Events of levels 13 to 16 are predicted. Function $b(t)$ is calculated with $\Delta = 20$ for levels 7 to 12.

Fig. 11 The global magnitude-frequency relationship, calculated for the time interval $T = (0 - 40000)$ for events of direction e_1 — (1), and direction e_2 – – (2). Parameters of the model are the same as for Fig. 10. Levels 3 to 14 are retained in the computation.

Allègre, C. J. and Le Mouël, J. L., 1994. Introduction of scaling techniques in brittle frittle fracture of rocks. *Phys. Earth Planet. Int.*, **87**, 85-93.

Allègre, C. J., J. L. Le Mouël, and Provost, A., 1982, Scaling rules in rock fracture and possible implications for earthquake prediction, *Nature*, **297**, 47-49.

Allègre, C. J., J. L. Le Mouël, Ha Duyen Chau and Narteau, C., 1995, Scaling organization of fracture tectonics (SOFT) and earthquake mechanism, *Phys. Earth Planet. Int.*, **92**, 215-233.

Bak, P., Tang, C. and Wiesenfield, K., 1988, Self-organized criticality, *Phys. Rev. A*, **38**, 364-374.

Bak, P. and Tang, C., 1989, Earthquakes as a self-organized critical phenomenon, *J. Geophys. Res.*, **94**, 15635-15637.

Barriere, B. and Turcotte, D. L., 1994, Seismicity and self-organized criticality, *Phys. Rev. E*, **49**, 1151-1160.

Blanter, E. M. and Shnirman, M. G., 1996, Self-organized criticality in hierarchical model of defects development, *Phys. Rev. E.*, **53**, 3408-3416.

Blanter E. M., Shnirman M. G., Le Mouël J. L. and Allègre C. J., 1996, Scaling laws in blocks dynamics and dynamic self-organized criticality, *Phys. Earth Planet. Int.*, **99**, 295-307.

Keilis-Borok V. I. and Rotwain I. M., 1990, Diagnosis of time of increased probability of strong earthquakes in different regions of the world: algorithm CN,*Phys. Earth Planet. Int.*, **61**, 57-72.

Keilis-Borok V. I. and Kossobokov V. G., 1990, Premonitory activation of earthquake flow: algorithm M8, *Phys. Earth Planet. Int.*, **61**, 73-83.

Molchan G. M., 1991, Structure of optimal strategies in earthquake prediction, *Tectonophysics*, **193**, 267-276.

Narkunskaya G. S. and Shnirman M. G., 1994, On an Algorithm of Earthquake Prediction, *Computational Seismology and Geodynamics*, **Vol.1**, 20-25 (American Geophysical Union, Washington, D.C.)

Novikova O. V. and Rotwain I. M., 1996, Experience of forward earthquake prediction with CN algorithm, Doclady RAN, **348**, 548-551, (in Russian).

Olami Z., Feder H. and Christensen K., 1992, Self-organized criticality in a non-conservative cellular automaton modeling earthquakes, *Phys. Rev. Lett.*, **68**, 1244-1247.

Pepke S. L. and Carlson J. M., 1994, Predictability of Self-Organizing Systems, *Phys. Rev. E*, **50**, 236-242.

Rotwain I. M. (personal communications).

Shaw B., Carlson J. and Langer J., 1992, Patterns of seismic activity preceding large earthquakes, *J. Geophys. Res.*, **97**, 479-488.

Socolar J., Grinstein G. and Jayaprakash C., 1993, On self-organized criticality in nonconserving systems, *Phys. Rev. E*, **47**, 2366-2376.

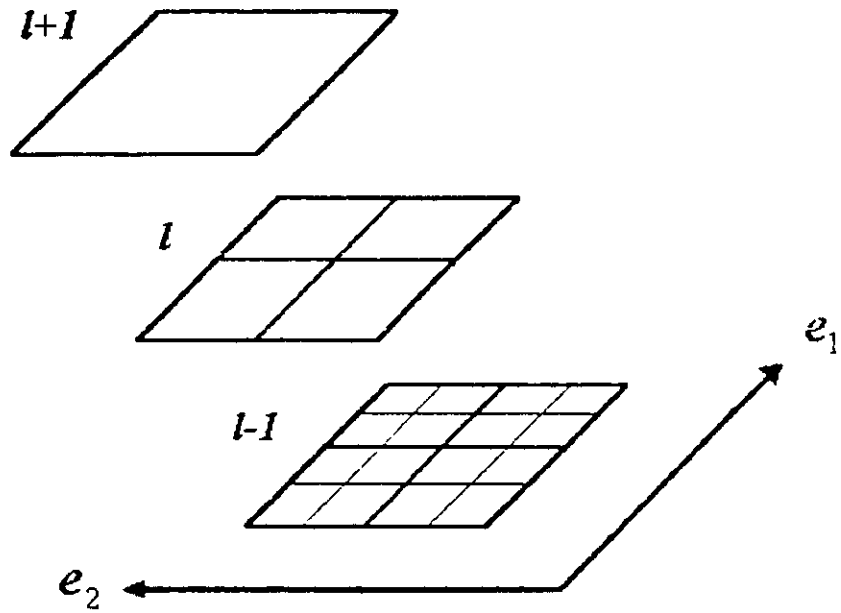
l+1
l
l-1
e_1
e_2

Fig 1

a)

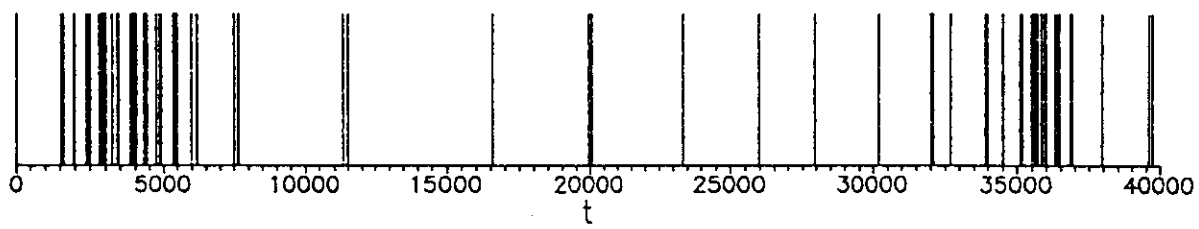
0
5000
10000
15000
20000
25000
30000
35000
40000
t

b)

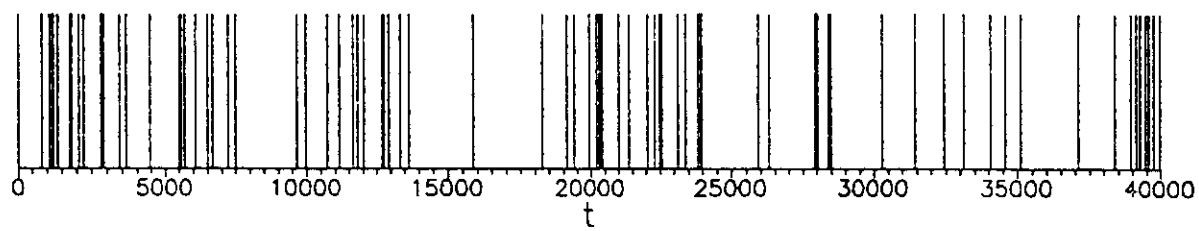
0
5000
10000
15000
20000
25000
30000
35000
40000
t

Fig 2

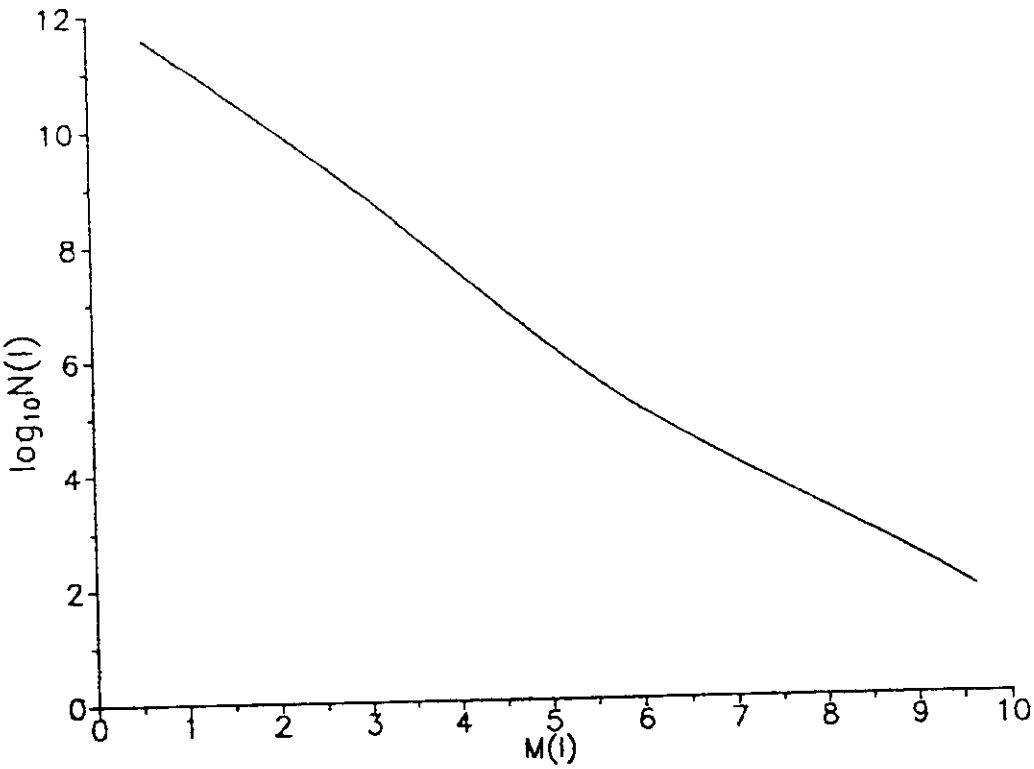
12
10
8
6
4
2
0
$\log_{10}N(I)$
0 1 2 3 4 5 6 7 8 9 10
M(I)

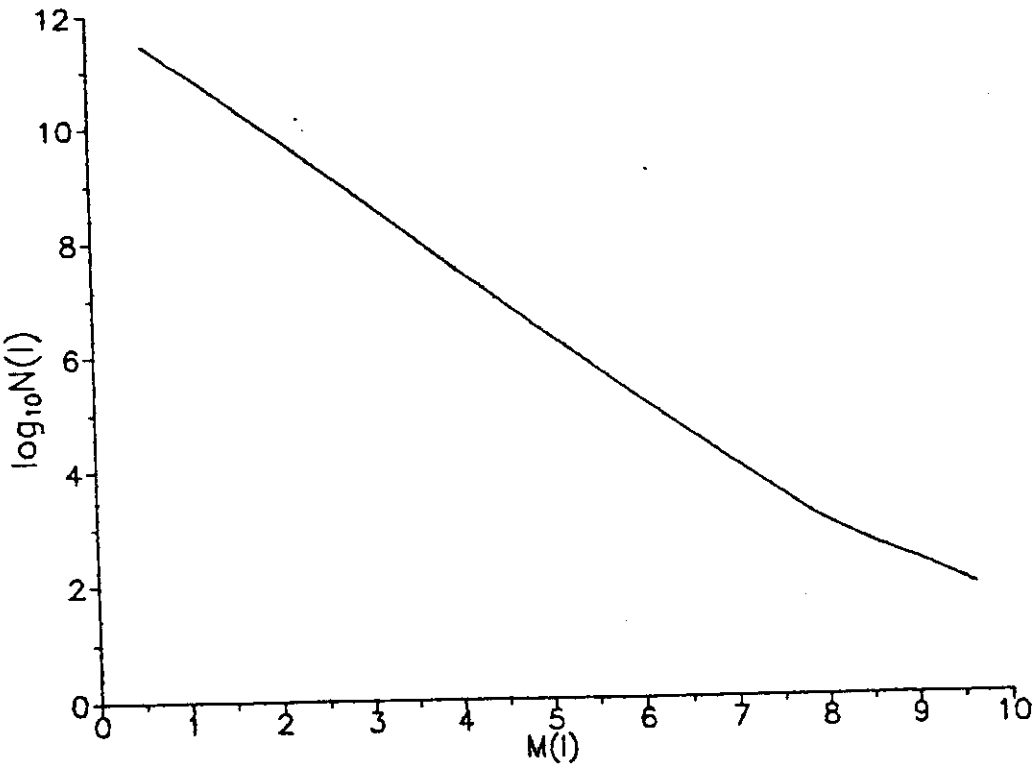
12
10
8
6
4
2
0
$\log_{10}N(I)$
0 1 2 3 4 5 6 7 8 9 10
M(I)

Fig 3 a, b

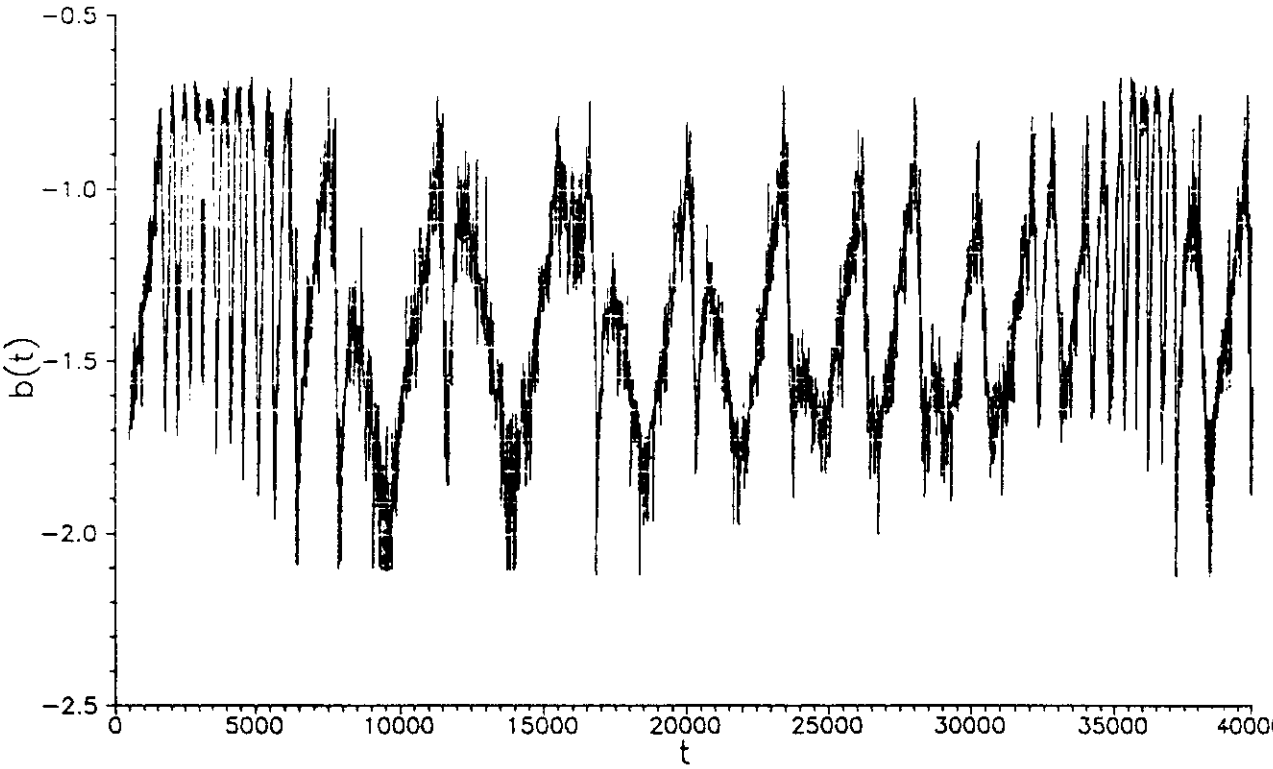
−0.5
−1.0
−1.5
−2.0
−2.5
b(t)
0
5000
10000
15000
20000
25000
30000
35000
40000
t

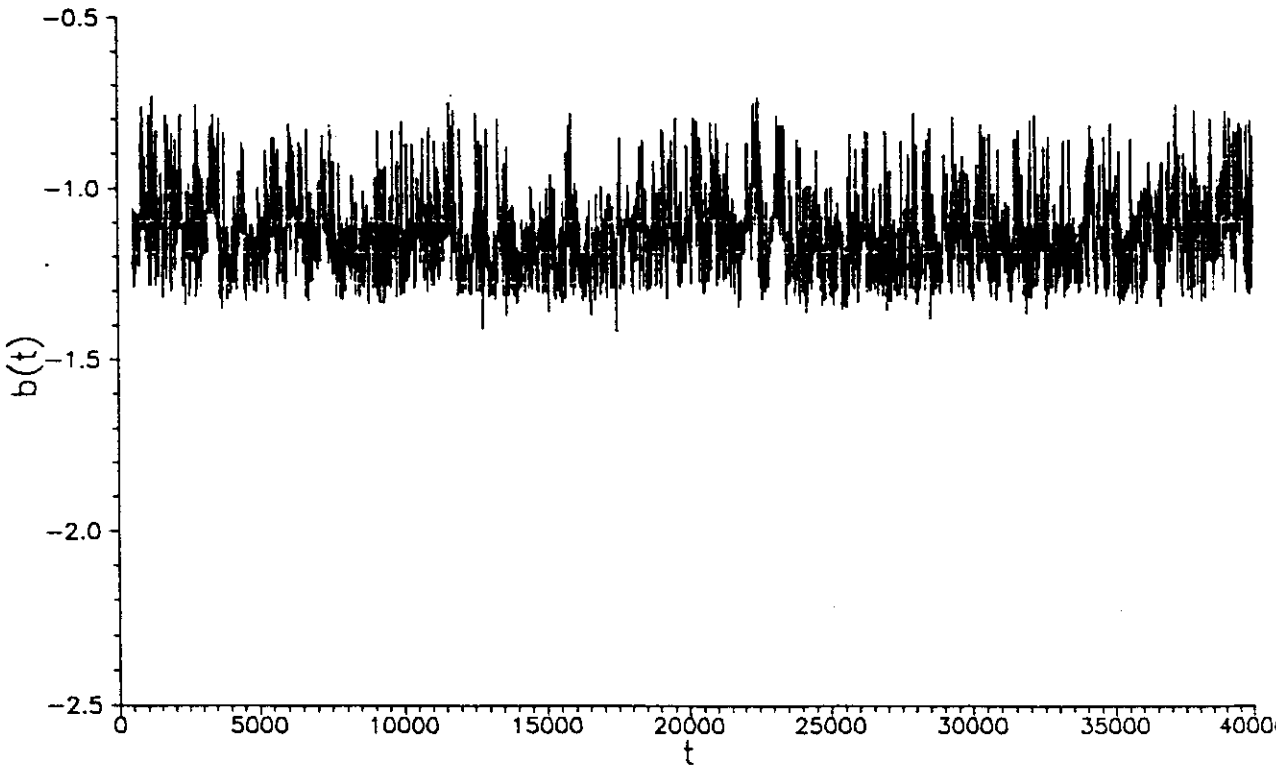
−0.5
−1.0
−1.5
−2.0
−2.5
b(t)
0
5000
10000
15000
20000
25000
30000
35000
40000
t

Fig 4 a, b

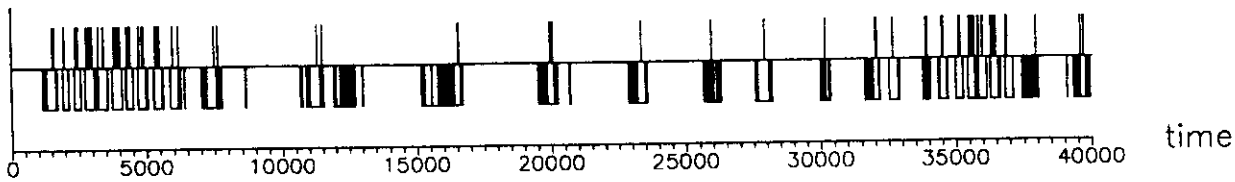
0
5000
10000
15000
20000
25000
30000
35000
40000
time

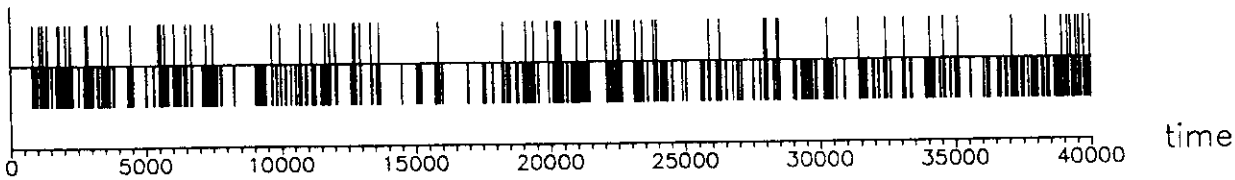
0
5000
10000
15000
20000
25000
30000
35000
40000
time

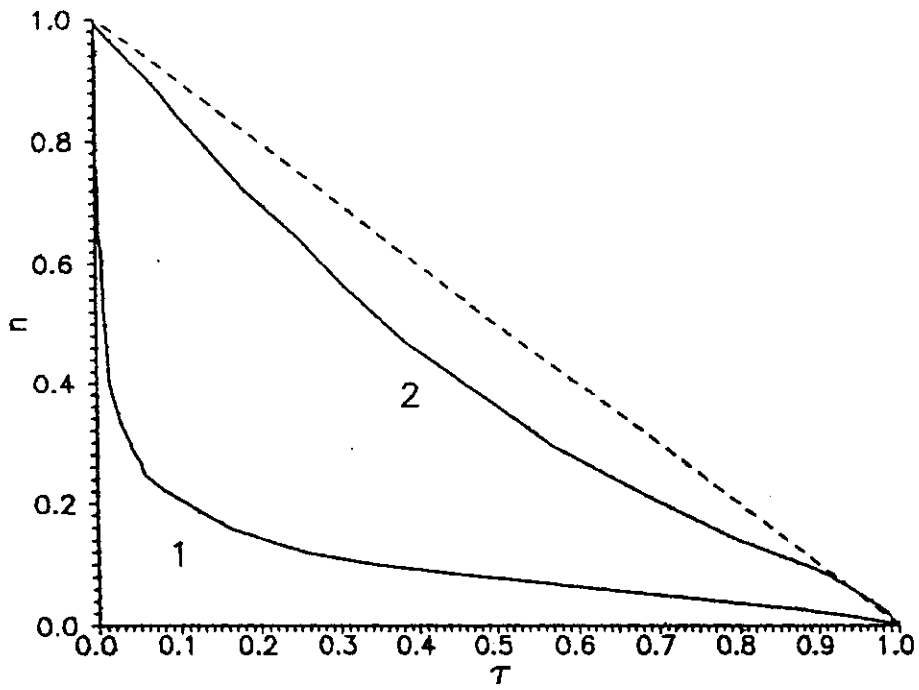
1.0
0.8
0.6
0.4
0.2
0.0
n
2
1
0.0 0.1 0.2 0.3 0.4 0.5 0.6 0.7 0.8 0.9 1.0
τ

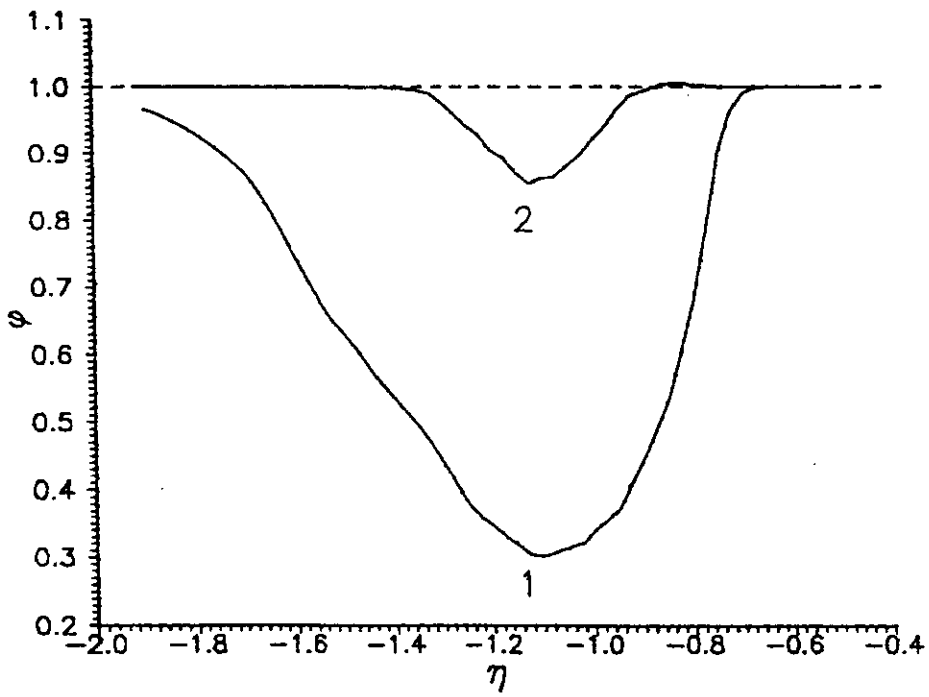
1.1
1.0
0.9
0.8
0.7
0.6
0.5
0.4
0.3
0.2
φ
2
1
−2.0 −1.8 −1.6 −1.4 −1.2 −1.0 −0.8 −0.6 −0.4
η

Fig 6 a, b

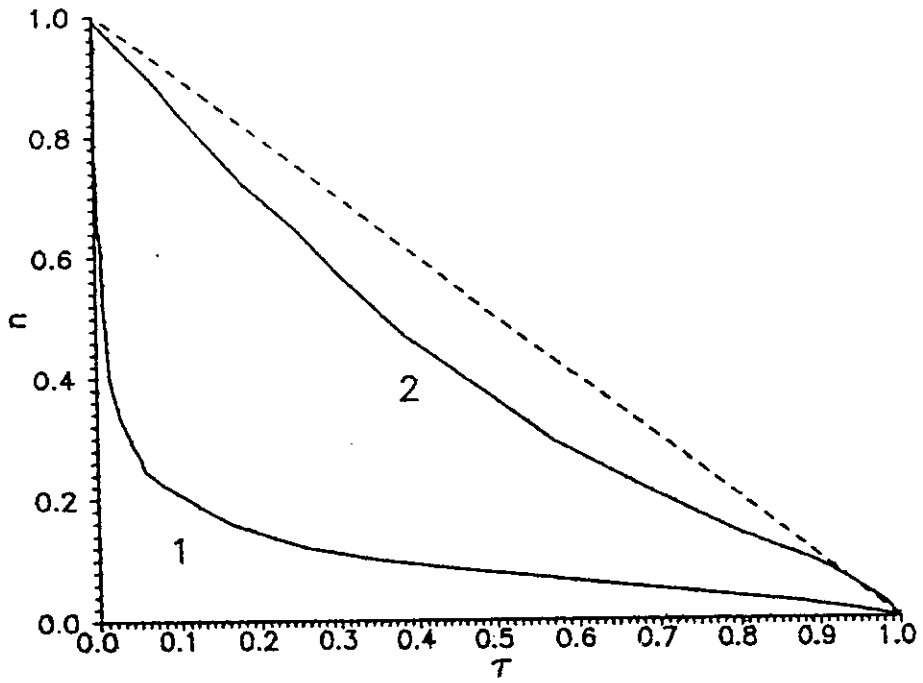
1.0
0.8
0.6
0.4
0.2
0.0
c
2
1
0.0 0.1 0.2 0.3 0.4 0.5 0.6 0.7 0.8 0.9 1.0
τ

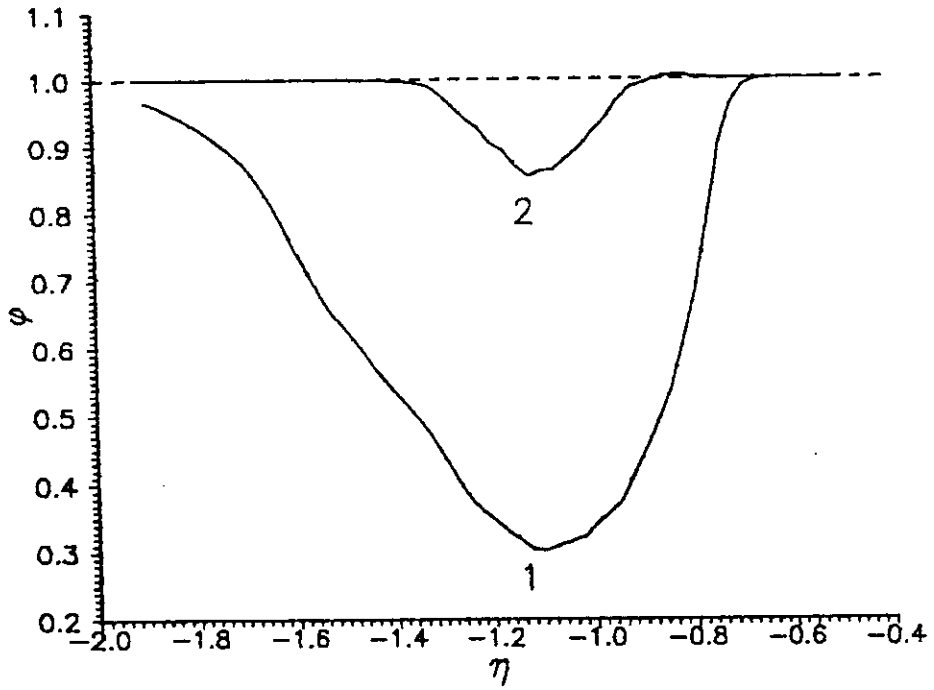
1.1
1.0
0.9
0.8
0.7
0.6
0.5
0.4
0.3
0.2
s
2
1
−2.0 −1.8 −1.6 −1.4 −1.2 −1.0 −0.8 −0.6 −0.4
η

Fig 6 a, b

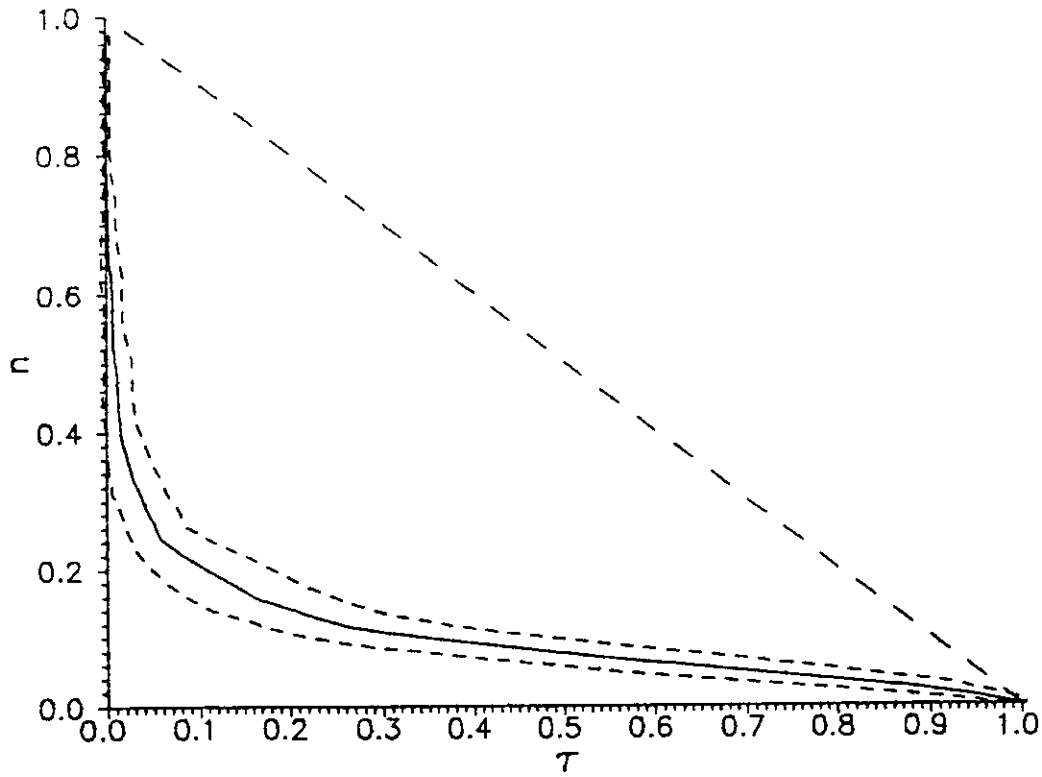
1.0
0.8
0.6
0.4
0.2
0.0
n
0.0 0.1 0.2 0.3 0.4 0.5 0.6 0.7 0.8 0.9 1.0
τ

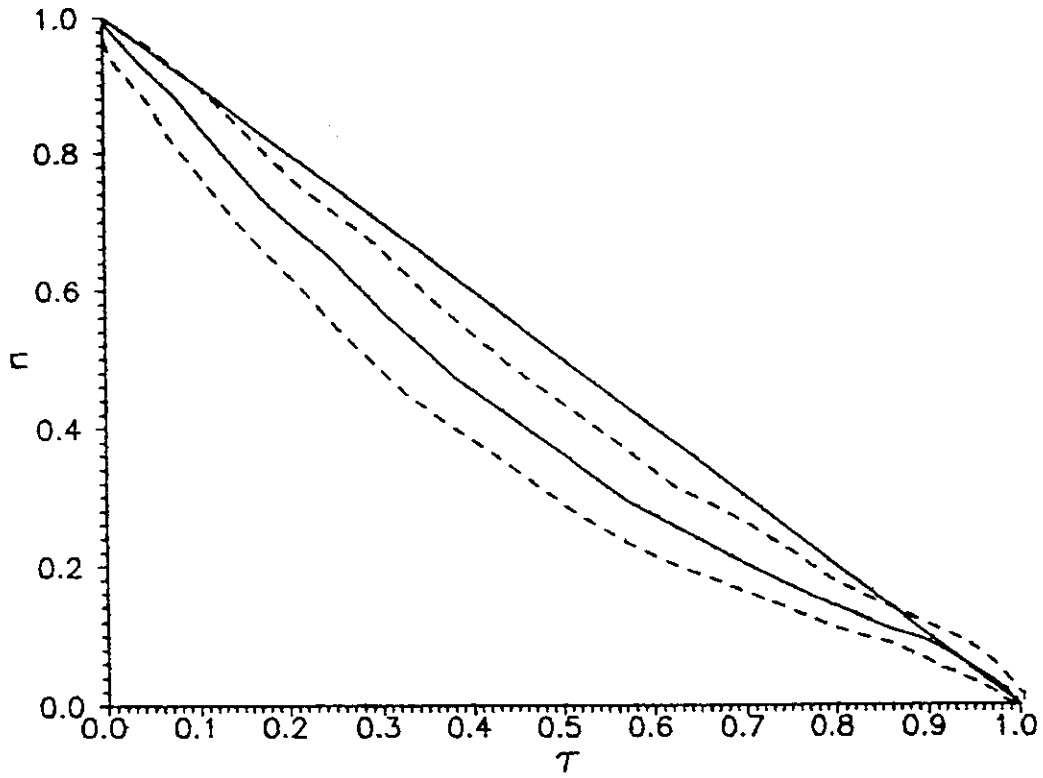
1.0
0.8
0.6
0.4
0.2
0.0
n
0.0 0.1 0.2 0.3 0.4 0.5 0.6 0.7 0.8 0.9 1.0
τ

Fig 7 a, b

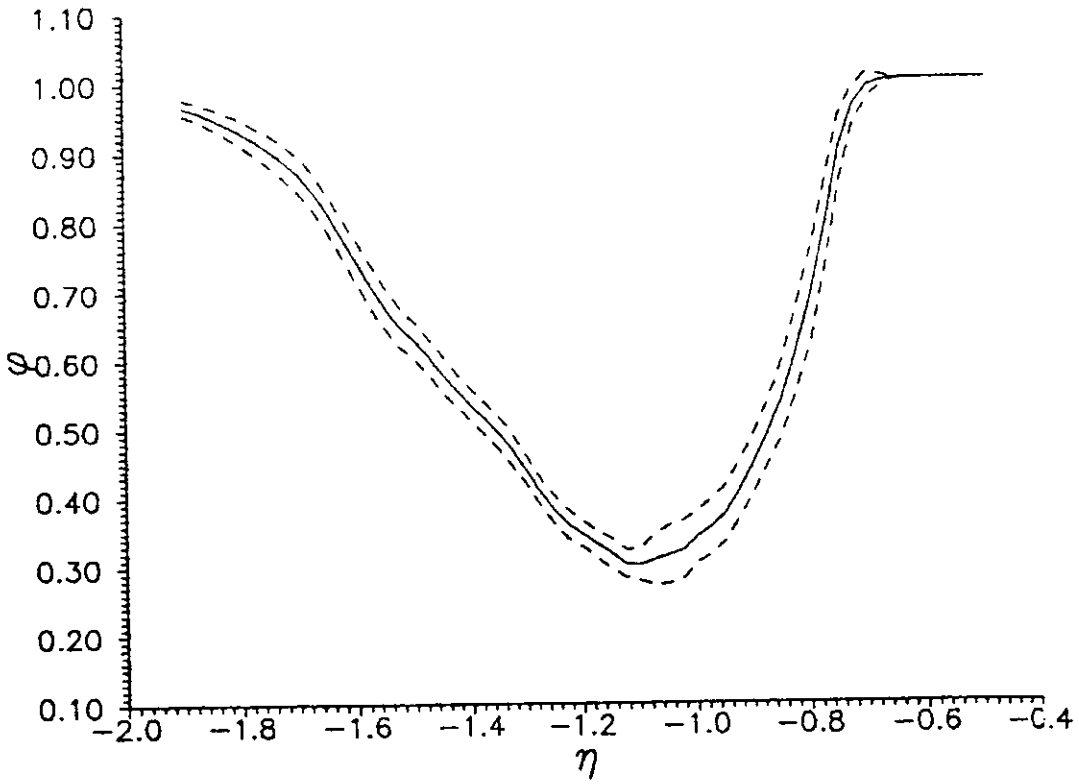
1.10
1.00
0.90
0.80
0.70
0.60
0.50
0.40
0.30
0.20
0.10
S
−2.0
−1.8
−1.6
−1.4
−1.2
−1.0
−0.8
−0.6
−0.4
η

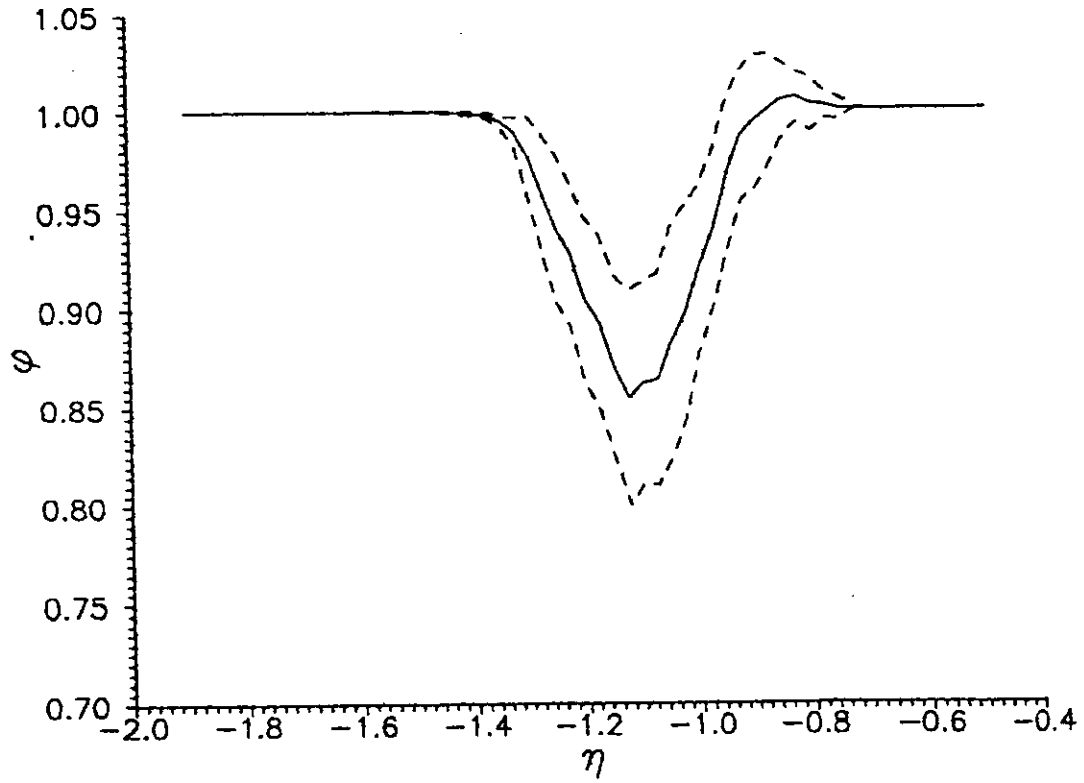
1.05
1.00
0.95
0.90
0.85
0.80
0.75
0.70
S
−2.0
−1.8
−1.6
−1.4
−1.2
−1.0
−0.8
−0.6
−0.4
η

Fig 8 a, b

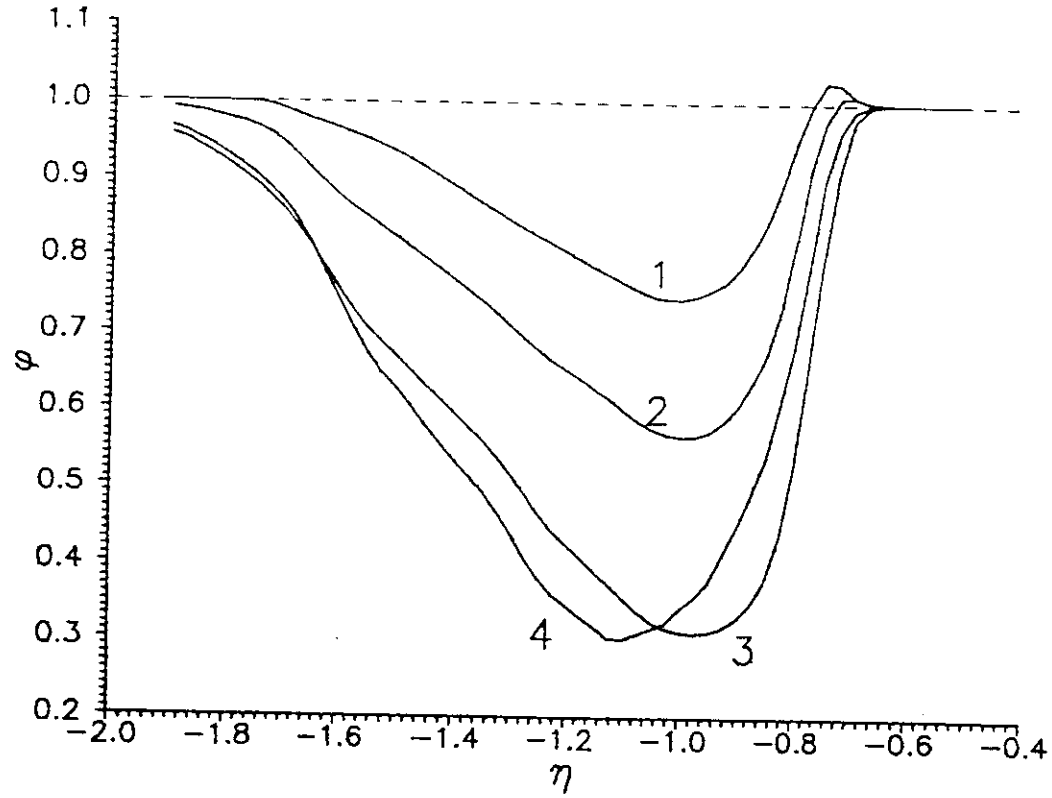
1.1
1.0
0.9
0.8
0.7
φ
0.6
0.5
0.4
0.3
0.2
−2.0
−1.8
−1.6
−1.4
−1.2
−1.0
−0.8
−0.6
−0.4
η
1
2
3
4

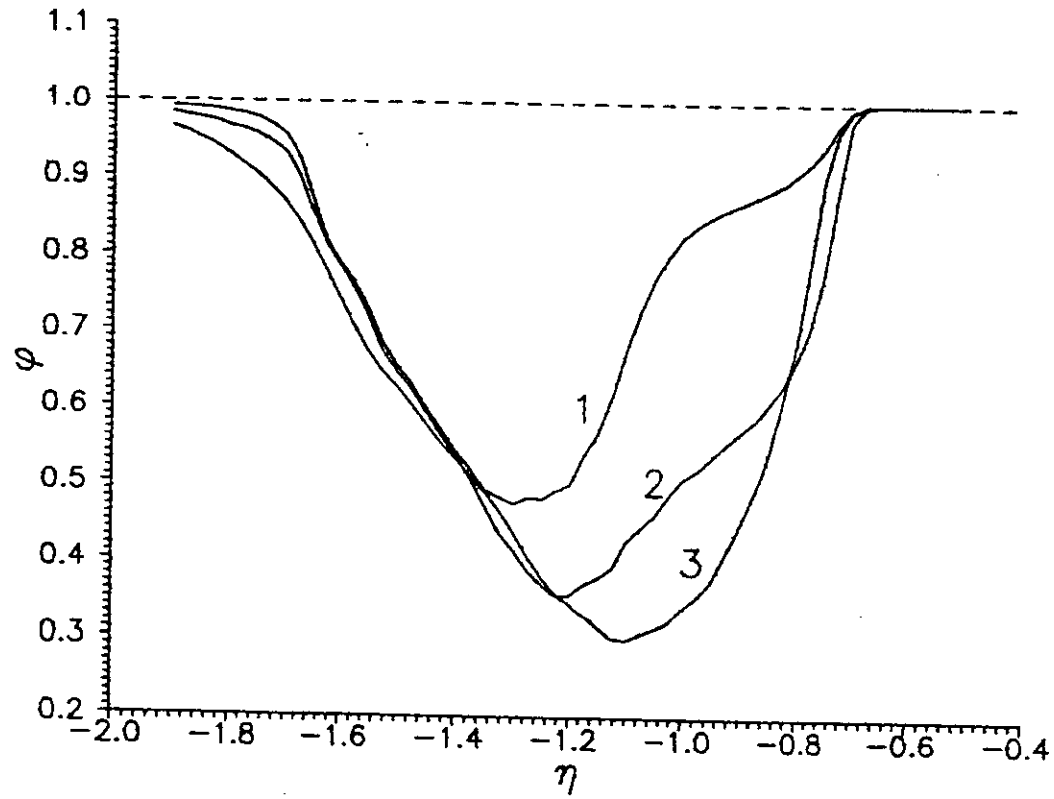
1.1
1.0
0.9
0.8
0.7
φ
0.6
0.5
0.4
0.3
0.2
−2.0
−1.8
−1.6
−1.4
−1.2
−1.0
−0.8
−0.6
−0.4
η
1
2
3

Fig 9 a, b

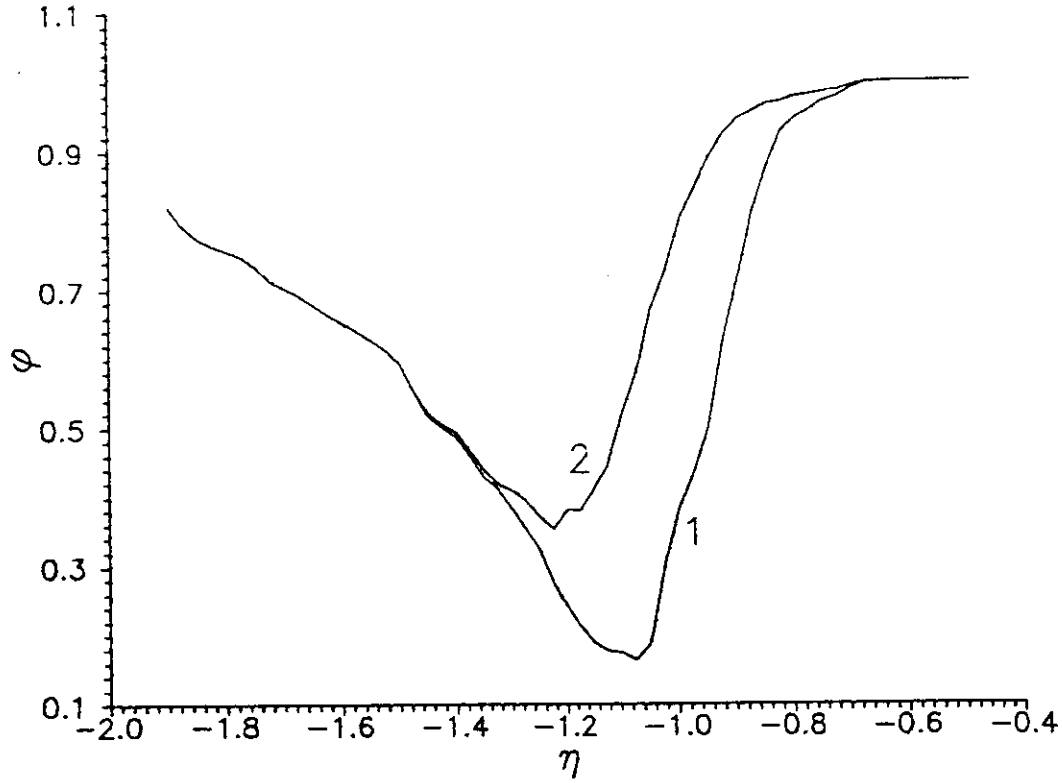
1.1
0.9
0.7
0.5
0.3
0.1
φ
2
1
−2.0
−1.8
−1.6
−1.4
−1.2
−1.0
−0.8
−0.6
−0.4
η

Fig 10

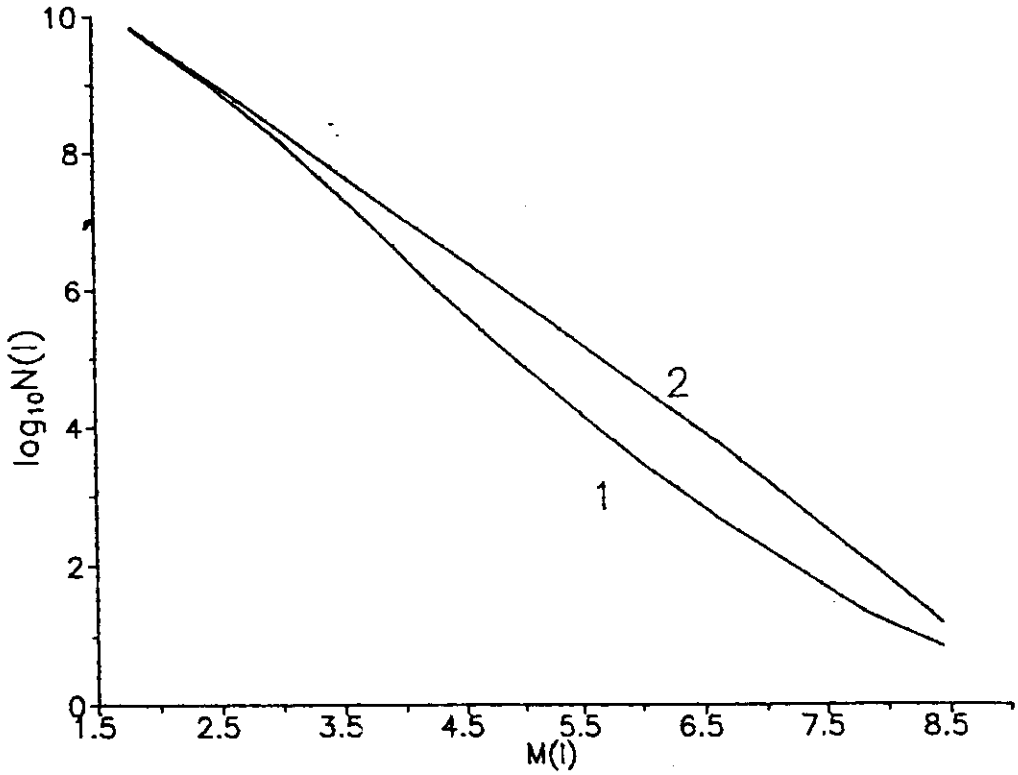
10
8
6
4
2
0
log₁₀N(l)
2
1
1.5
2.5
3.5
4.5
5.5
6.5
7.5
8.5
M(l)

Fig 11